Environmental Design Space Model Assessment

by

Phillip Michael Spindler
B.S. Aerospace Engineering
Purdue University, 2005

Submitted to the Department of Aeronautics and Astronautics
in partial fulfillment of the requirements for the degree of

Master of Science in Aeronautics and Astronautics

at the

MASSACHUSETTS INSTITUTE OF TECHNOLOGY

May 2007
[June 2007]

Author .....
Department of Aeronautics and Astronautics
May 23, 2007

Certified by .....
Ian A. Waitz
Jerome C. Hunsaker Professor of Aeronautics and Astronautics
Thesis Supervisor

Accepted by .....
Jaime Peraire
Professor of Aeronautics and Astronautics
Chair, Committee on Graduate Students

Environmental Design Space Model Assessment

by

Phillip Michael Spindler

B.S. Aerospace Engineering

Purdue University, 2005

Submitted to the Department of Aeronautics and Astronautics
on May 23, 2007, in partial fulfillment of the
requirements for the degree of
Master of Science in Aeronautics and Astronautics

Abstract

The Environmental Design Space (EDS) is a multi-disciplinary design tool used to explore trade-offs among aircraft fuel burn, emissions, and noise. This thesis uses multiple metrics to assess an EDS model of a Boeing 777 aircraft. Starting from a detailed description of the EDS framework, a description of EDS model creation is outlined. The aircraft and engine model is assessed by a comparison to an industry-developed model and changes to the EDS model are explored to improve the model's predictive ability. The model is assessed by sensitivity studies on the inputs, component performance maps, and constraints. An alternate method of applying additional constraints to EDS results is also investigated. Finally, the model uncertainty is quantified using Monte Carlo simulations. This includes a study where all the inputs are varied and a study which investigates the implications of model uncertainty on trade study results.

The comparison to the industry model shows that optimization around three design points is required to develop a model of acceptable accuracy. The input sensitivity study shows that there are only a few key drivers to the EDS model, but the direction of the trends with some of these variables is counterintuitive due to the typical practice constraint of holding the aircraft thrust to weight ratio constant. The constraint sensitivity study reveals there are only a handful of constraints implemented in EDS and the current method for applying additional constraints can increase the resultant errors due to the response surfaces generated. The uncertainty studies reveal the implications of attempting to correct cases which would otherwise fail and how fixes can skew results and increase uncertainty. Finally, the trade study uncertainty analysis shows that EDS is capable of answering questions with higher confidence than one would assume from the results of the input uncertainty study since the uncertainty due to variables which are not changing in a trade study are not significant.

Thesis Supervisor: Ian A. Waitz
Title: Jerome C. Hunsaker Professor of Aeronautics and Astronautics

Acknowledgments

I would like to first thank my advisor, Professor Ian Waitz, who made it possible for me to study at MIT and who guided me through this research. Professor Karen Willcox's insight into complex problems helped me greatly with the uncertainty analysis. I would also like to thank Joe Palladino, whose wealth of knowledge was a great asset any time I needed guidance.

A special thanks to my friends in the Gas Turbine Lab; Andrew March, Bastien Martini, Julien Rojo, and Tim Yoder who were around to bounce ideas off of and made every day in the lab a bit more fun. Also, my friends Andrew and Caroline Lamb and Andy and Liz Copeland for adopting my wife and me as family since we were far from our own.

Finally, I would like to thank my wife Megan for moving across the country with me a few times and for not complaining too much when I ask her to proof read my writing. Also, I want to thank the rest of my family for their love and support.

This work was supported by the Office of Environment and Energy, U.S. Federal Aviation Administration under Cooperative Agreement No. 03-C-NE-MIT, Amendment Nos. 011, 015, 018, 022, and 025. The effort was managed by Joseph DiPardo. Any opinions, findings, and conclusions or recommendations expressed in this material are those of the author and do not necessarily reflect the views of the FAA.

Contents

List of Figures

List of Tables

Nomenclature

AEDT	Aviation Environmental Design Tool
ANOPP	Aircraft Noise Prediction Program
APMT	Aviation Environmental Portfolio Management Tool
BPR	Bypass Ratio
CAEP	Committee on Aviation Environmental Protection
EDS	Environmental Design Space
EPNL	Effective Perceived Noise Level
FAR	Federal Aviation Regulation
FLOPS	Flight Optimization System
FPR	Fan Pressure Ratio
GEAE	General Electric Aircraft Engines
HPC	High Pressure Compressor
HPT	High Pressure Turbine
ICAO	International Civil Aviation Organization
LPC	Low Pressure Compressor
LPT	Low Pressure Turbine
LTO	Landing and Takeoff Cycle
LTO-NO_x	Nitrous Oxides emitted during the landing-takeoff cycle
NOx	Nitrous Oxides
NPSS	Numerical Propulsion System Simulation
OPR	Overall Pressure Ratio
PW	Pratt and Whitney
SLS	Sea-level static
T4	Turbine Inlet Temperature
TO	Takeoff
TOC	Top of Climb
TSFC	Thrust Specific Fuel Consumption
V_{jet}	Ratio of engine core exhaust to bypass exhaust velocity
WATE	Weight Analysis of Turbine Engines

Chapter 1

Introduction

1.1 Motivation

The Environmental Design Space (EDS) is a suite of tools being developed to explore trade-offs among aircraft fuel burn, emissions, and noise. EDS provides input to the Aviation Environmental Porfolio Management Tool (APMT) which is used to assess operational, policy, and market scenarios for current and future aircraft. Since these tools will be used for policy making decisions, model assessment is an important part of the development process. One of the first steps taken to assess EDS was to compare it with industry accepted results. Comparing performance trends generated by EDS with those generated by Pratt & Whitney provides a way of assessing EDS's engine design method and its ability to accurately capture performance changes for various engine designs.

It is also important to investigate the effect of changing all the inputs and constraints that are implemented in the model. Due to the highly complex nature of multidisciplinary design tools, such as EDS, the effect of changing inputs is not necessarily what one would expect. These effects are investigated using sensitivity studies on both the inputs and constraints.

EDS is comprised of five independent modules and each of those modules has subelements with their own assumptions and approximations. When these modules are combined to predict aircraft fuel burn, emissions, and noise, the various assump-

tions and approximations combine, creating uncertainty. Since EDS is intended to give information about making policy decisions, it is important to understand the system level uncertainty. For example, consider a prediction used to evaluate which aircraft an airline would purchase to add to their fleet. Assuming that the policy scenario under study is met, the airline would pick the most cost effective aircraft which is most likely to be the aircraft with the highest fuel efficiency. In a competition where the differences between aircraft are very slim, the uncertainty of fuel burn predictions in EDS may cause the scales to tip one way or another. This uncertainty in EDS stems from two sources; uncertainty due to the computational methods used in the model and uncertainty due to lack of knowledge of the inputs. The first type of uncertainty is often caused by tolerances implemented in the design tool solution methods. Uncertainty due to lack of knowledge of the inputs is investigated using Monte Carlo simulations.

1.2 Thesis Objectives

The objectives of this thesis are to:

- Compare EDS with Pratt & Whitney preliminary design tools.
- Assess EDS input and constraint sensitivity.
- Assess EDS uncertainty via a probabilistic approach.
- Evaluate EDS's ability to calculate high confidence results for typical policy scenarios.

1.3 Previous Work

Computational models, being the basis for system performance prediction, are a crucial element of engineering design[14]. The credibility of these computational models is of great importance to both decision makers and those who are affected by the decisions made based on these predictions because of the high potential cost[27]. The

process of evaluating model credibility is termed verification and validation. Verification is the process of confirming that a computational model correctly implements the algorithms that were intended and evaluates the extent to which the model or simulation has been developed using sound and established software engineering techniques. Validation is the process of confirming that the predictions of a computational model adequately represent measured physical phenomena or other accepted results[10][17].

Uncertainty quantification is becoming an increasingly important part of the verification and validation process and it is a problem that many people are continuing to study. One of the most common ways to address uncertainty is through uncertainty propagation which strives to predict output uncertainty distributions based on input uncertainties[28]. The first step to approach uncertainty quantification is to identify all the avenues of uncertainty in the simulation, which may include uncertainties in approximate models for they underlying physics, approximations in numerical algorithms, and uncertainty in the model inputs[5]. Once this is established, a sensitivity analysis must be used to determine which components of uncertainty are the major drivers of the output metrics[20]. Sensitivity analysis involves determination of the amount and kind of change produced in a given model output by a change in model input and is important in determining the system response[26].

To perform a sensitivity study to filter out the components of uncertainty that are not dominant, one must determine acceptable bounds of uncertainty for the inputs of the model. The determination of physically reasonable bounds requires a considerable research effort in itself and the quantification of these bounds may be possible using information from experiments, analytic analysis and scientific or engineering judgment. These uncertainties are propagated through the simulation model using methods such as Monte Carlo simulations to determine a predictable total output uncertainty in the model response to variation of the inputs. When performing Monte Carlo simulations, the model is run for a series of related cases. Unfortunately, it is a common feature of complex analysis codes that there are frequent case failures when run in this situation[12]. If these failures are any way correlated to the input variations, they can lead to skewed output uncertainty distributions.

1.4 Outline

This chapter introduced the idea of EDS and the thesis objectives. Chapter 2 provides an overview of EDS, the modules used in EDS, and how EDS fits into the larger APMT environment. This is followed by a description of the aircraft-engine model creation and assessment by comparison with results from Pratt & Whitney in Chapter 3. Chapter 4 outlines the assessment process, including variable and distribution selection. In addition, a number of studies are performed to evaluate the design tool uncertainty. The thesis ends with Chapter 5 reviewing the major points and suggesting future development.

It should be noted that the baseline aircraft for all the studies is a 300 passenger wide-bodied aircraft with a range of 8100 nmi which closely approximates the Boeing 777-200. The engine model is a Pratt & Whitney 4000 112" diameter turbofan.

Chapter 2

EDS Overview

2.1 Introduction

This chapter starts with an overview of how the Environmental Design Space (EDS) provides input to the Aviation Environmental Portfolio Management Tool (APMT). A description of the EDS framework is then given followed by an overview of the computational modules in EDS.

2.2 APMT

The Federal Aviation Administration's (FAA) Office of Environment and Energy (AEE), in collaboration with the National Aeronautics and Space Administration (NASA), is developing a tool to assess the local and global effects of the aviation market. APMT will be used to evaluate relationships among aircraft noise, emissions, and cost valuations[29]. APMT encompasses four major subcomponents; EDS, the Demand and Supply Projection (DSP), the Benefits Valuation Block (BVB), and the Aviation Environmental Design Tool (AEDT), which are shown in Figure 2-1.

The policy scenario under investigation is input to APMT which requires EDS to perform aircraft system level trades and technology forecasting. After running the aircraft from EDS through an operations generator, which simulates airline supply and demand relationships, the fleet level data are passed to AEDT which computes global

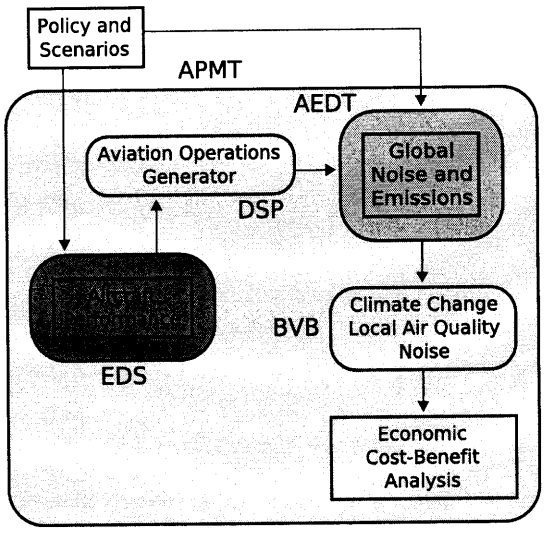

Figure 2-1: Aviation Environmental Portfolio Management Tool

emissions and noise. These global emissions and noise results are then propagated to determine impact on climate change, local air quality, and noise. APMT then performs a cost-benefit analysis to sum up the environmental and economic impacts.

2.3 EDS

EDS provides the vehicle level analysis for APMT which subsequently simulates a fleet of aircraft to provide economic and environmental impacts. The goal of EDS is to assess source noise, exhaust emissions, and performance parameters for current and future aircraft designs under various policy and market scenarios. EDS incorporates five NASA simulation modules to calculate these various attributes. More than a simulation code itself, EDS is a framework to perform aircraft system level trades and technology forecasting.

EDS is able to automatically run through all the cases in a design of experiments table. Figure 2-2 shows a high-level flowchart EDS runs through for each case in the design of experiments. EDS starts by creating input files for the Numerical Propulsion System Simulation (NPSS) module based on the data in the design of experiments table. The engine scale factor is set to one for the initial run through the engine

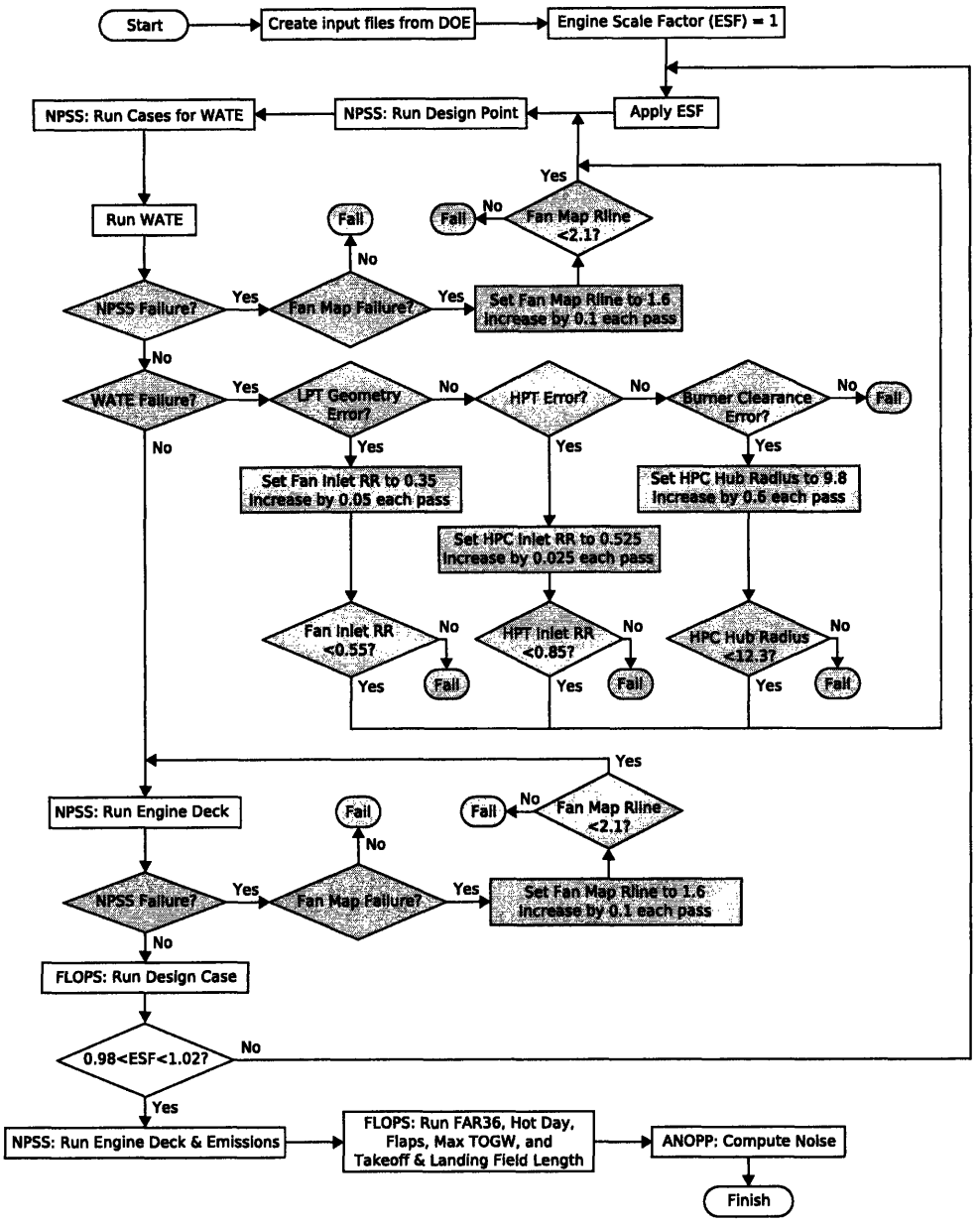

Figure 2-2: EDS Framework Flow Path - White boxes are the main program flow and shaded boxes are error correction steps.

sizing loop. The engine sizing loop matches the engine thermodynamics computed by NPSS and the engine weight computed by the Weight Analysis of Turbine Engines (WATE) module with the engine size required to fly the mission computed by the Flight Optimization System (FLOPS). NPSS analyzes the engine design point (for this thesis the design point is sea level static condition) and sizes the bypass nozzle area for optimal thrust specific fuel consumption during cruise. NPSS also runs the engine at specific conditions for use by WATE. After WATE computes the engine weight, EDS checks the output from both NPSS and WATE to look for errors. If NPSS can not converge on the engine thermodynamic cycle because there is a problem with the fan component map, EDS attempts to fix the error by changing the operating location on the fan map. If an error in WATE is found, EDS checks to see if the error is due to LPT geometry, HPT failure, or a burner clearance error. If the NPSS runs can not converge after EDS attempts to fix the problem, the case fails and EDS moves on to the next point in the design of experiments.

If NPSS and WATE run correctly, NPSS is run again to compute the engine deck. FLOPS runs the design point and computes a new engine scale factor. FLOPS varies gross takeoff weight and engine size to hit a target thrust to weight ratio and a target range. If the engine scale factor is not between 0.98 and 1.02, meaning the max thrust of the engine NPSS computed is more than 2% off the size engine that FLOPS needs, EDS scales the engine NPSS calculates and starts the entire flow over. If the engine scale factor is sufficiently close to one, EDS continues on to compute more engine decks for FLOPS and runs the engine at specific points to compute LTO-NO_x emissions. FLOPS then runs off-design cases including flight plans to compute aircraft noise and takeoff and landing field lengths. Finally, the aircraft-engine noise is computed using the Aircraft Noise Prediction Program (ANOPP).

2.3.1 Engine Cycle Module, NPSS

The Numerical Propulsion System Simulation software is an object-oriented programing framework and analysis package developed by NASA's Goddard Research Center and a number of industry partners including major engine and airframe

manufacturers[24]. The NPSS framework allows for integration of various computational models in the hopes of reducing product development time and reducing the need for full-scale testing. The NPSS turbofan engine model is assembled from a number of different interconnected components as shown in Figure 2-3. The model begins with ambient conditions which are fed into the fan. The fan and the low pressure compressor (LCP) are physically connected to the low pressure spool and powered by the low pressure turbine (LPT). There is a splitter directly after the fan which separates the bypass flow from the core flow. The bypass flow passes through a duct to bypass nozzle. The core flow continues to the LPC and high pressure compressor (HPC). The high pressure compressor is powered off the high pressure shaft by the high pressure turbine (HPT). Two cooling flows are removed from the core flow directly after the compressor to cool the HPT and LPT. After the cooling flow is removed, the core flow continues through the burner, HPT, LPT, and on to the core nozzle.

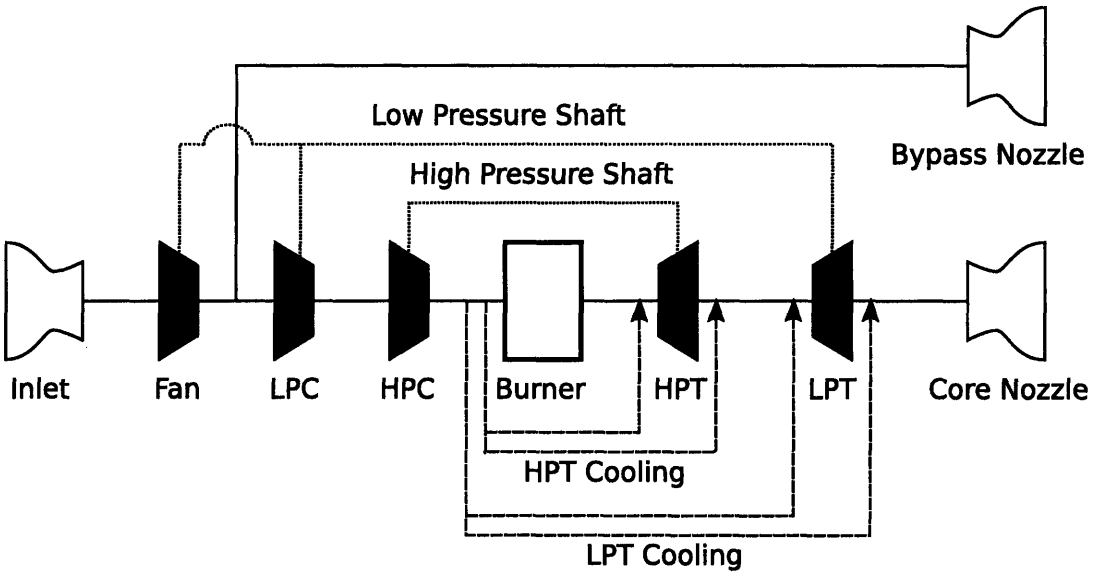

Figure 2-3: NPSS Engine Flow Path Example

The component maps are parametrically generated during the model creation phase using three NASA codes; MODFAN[8], CMPGEN[6], and PART[7]. Once a model baseline is created, the component map scaling is done within NPSS where

map scale factors are calculated using the design case (sea-level static conditions at maximum power for the models used herein) and applied to the map for use at off-design points. MODFAN is used to generate fan compressor maps and CMPGEN is used to generate the low pressure and high pressure compressor maps. MODFAN and CMPGEN both use design pressure ratio, design inlet corrected flow, and stall margin to generate tables of pressure ratio, corrected flow, and efficiency for various corrected speeds and pressure ratio parameters. The component map data is generated using semi-empirical relations based on parameters derived from the basic physics of the components. The LPT and HPT maps are generated using PART, a comparable program designed for turbine map generation.

The engine components are controlled by the NPSS solver which uses Newton-Raphson methods to ensure the engine is in a self-consistent, or converged, state. For the design case, NPSS iterates to meet the design exit velocity ratio and maximum turbine inlet temperature by varying the fuel to air ratio and the bypass ratio. Engine maximum thrust at any given altitude is computed by increasing the fuel to air ratio until the maximum LPT rotational speed it achieved. Off-design cases at part power are computed by varying the fuel to air ratio to achieve the target thrust.

2.3.2 Engine Weight Module, WATE

Originally developed by Boeing Military Aircraft Company in 1979 for use in the NASA Engine Performance Program, WATE estimates the component weight and dimensions of turbojet engines. Created with conceptual design in mind, the initial version of WATE relied heavily on empirical correlations. The current incarnation of WATE still includes some approximations based on empirical data and material properties but also includes higher fidelity calculations to compute sizes and weights for the engine inlet, compressors, turbines, burner, mixers, ducts, splitter, and nozzles.

EDS uses WATE to compute detailed engine component weights, sizes, and to implement structural limitations on the engine design. WATE varies the fan speed factor to meet a specified fan work factor. The number of LPC stages is computed to meet a specified maximum blade loading. The HPC rotational speed is computed

so to maintain a specified HPC work factor. The number of LPT stages is computed so the LPT inlet diameter is about 92% of the LPC inlet diameter. The core nozzle exit area is set to match 95% of the outer radius of the LPT. The bypass nozzle exit location is set to be about 300% of the fan's radius. There are also structural limitations implemented which maintain the disk stress levels below certain limits based on the type of disk geometry used.

2.3.3 Aircraft Performance Module, FLOPS

The Flight Optimization System (FLOPS) is a preliminary design tool which is used by EDS to calculate aircraft weights, aerodynamics, and mission performance[22]. Although FLOPS includes simple engine weight calculations, EDS imports that information from WATE. The aerodynamics module of FLOPS is based on an empirical drag buildup technique originally developed by Lockheed Martin[11]. FLOPS includes modifications to this method which smooth drag polars, include more accurate Reynolds number effects, and add skin friction calculations. EDS relies on FLOPS to predict cruise drag polars, but does not use FLOPS for the take off or landing drag polars. Specialized tools are used which incorporate the effect of flaps and slats in the low speed aerodynamics for the take off and landing drag polars. The mission performance module of FLOPS predicts performance of the aircraft-engine combination on the specified mission. In addition to calculating cruise performance, this module includes detailed calculations for the landing-takeoff (LTO) cycle to ensure the aircraft meets all FAR 25 requirements.

2.3.4 Emissions Module

EDS currently uses an empirical relation to compute NO_x emissions. The emissions investigations in this thesis focus on NO_x emitted during the landing-takeoff cycle (LTO-NO_x) which includes landing, taxi, takeoff, and climb out as shown in Figure 2-4. The LTO-NO_x is a weighted sum of the emissions indices during the four LTO segments given by,

$$NO_x = \sum_{i=mode} t_i \cdot \dot{m}_{f_i} \cdot EI_{NO_{x_i}} \tag{2.1}$$

where $\dot{m}_f$ is fuel flow, t is the segment time, and EI_{NO_x} is the NO_x emissions index. These segments represent the aircraft's activity when it is below 3000 ft altitude.

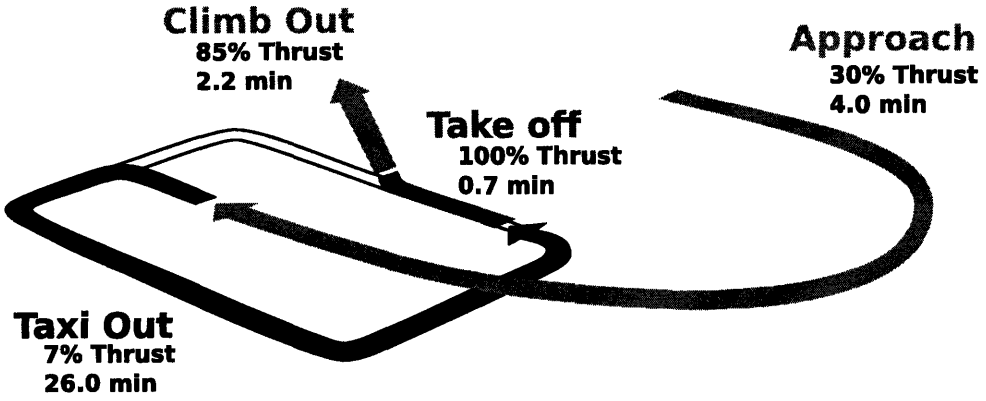

Figure 2-4: Thrust Settings and Segment Times to Measure Airport Emissions[9]

The emissions index for NO_x is based on a correlation between the burner entrance temperature and pressure given by,

$$EI_{NO_x} = 33.2 \left(\frac{P_{t3}}{432.7}\right)^{0.4} exp\left(\frac{T_{t3}-1487.27}{349.9} + \frac{6.29-1000*f_{humidity}}{53.2}\right)$$

where the subscript 3 denotes the burner entrance conditions, $f_{humidity}$ is an altitude dependent humidity factor, P is in psi and T is in R.

2.3.5 Aircraft Noise Prediction Module, ANOPP

The Aircraft Noise Prediction Program (ANOPP) was developed by NASA Langley Research Center as an empirical method of approximating aircraft noise. Since its inception in the 1970's, ANOPP has grown to be a well-known tool for predicting aircraft noise. ANOPP is made up of many modules, each of which perform specific noise calculations, such as computing noise for the fan, engine exhaust jet, or airframe. ANOPP has a history of over predicting noise. This over prediction has

been attributed to fan inlet noise which is predicted using the Heidmann model[15]. Recent advancements have been made from recommendations in past studies to improve ANOPP's noise prediction accuracy while maintaining the Heidmann model structure[21].

Chapter 3

Model Creation and Assessment

3.1 Introduction

This chapter outlines how EDS models are created and provides a side by side comparison of an EDS PW4090 engine model with initial design phase model results from Pratt & Whitney (PW). The motivations for the study are discussed, followed by the method used for the study. An overview of creating an EDS baseline model is described along with the differences between single and three point engine design methods. Finally, comparisons and conclusions are drawn from the EDS and PW results.

3.2 Motivation

One of the first steps in assessing EDS is to compare it with industry accepted results. It is important to be able to predict not only a single design point, but also to be able to predict trends with changes in design variables accurately. A number of studies have been performed already and many more are planned with the major aircraft and engine manufacturers including Pratt & Whitney, GE Aircraft Engines (GEAE), and Boeing.

EDS will provide a range of vehicle classes for use in policy making decisions. In order to remain transparent and available for use to a wide audience, EDS can not

include any proprietary information. Due to this, we approach the model assessment study not as a problem of matching the PW results exactly to every detail but as a task of evaluating if the PW design trends are captured correctly.

Since EDS will be used to evaluate policy scenarios, it is important to capture engine performance trends correctly. Comparing performance trends generated by EDS with those generated by PW provides a way of assessing EDS's engine design method and its ability to capture performance changes for various engine designs.

3.3 Method

This study is focused on the PW4090 engine flying on a Boeing 777-200 type aircraft for a 3000 nmi mission. The study begins with the creation of a new EDS model to represent this specific aircraft-engine combination. After an acceptable baseline is created, a design of experiments is conducted to assess engine performance trends. The resulting TSFC, mission fuel burn, bare engine weight, and LTO-NO_x emissions are monitored and results from EDS are compared to those generated using proprietary PW tools.

The design space is explored using a full factorial design of experiments that changes OPR by -5%/+17% of the baseline value and T4 by ±3% of the baseline value (from hereon the design space is nondimensionalized from 0 to 1). The overall pressure ratio is varied by changing the LPC pressure ratio, other engine parameters (such as FPR, HPC PR, and V_{jet}) are held constant throughout the design space. The engine is flown on a Boeing 777-200 type aircraft which has a design range of 8100 nmi but the results shown are for a more typical mission range of 3000 nmi. Since this study is intended to assess EDS's engine design methods, the aircraft is held fixed except for changes in weight due to the engine weight changing through the design space.

3.4 Model Creation

The process of creating a new engine model for EDS starts by collecting publicly available data on the engine from a number of different sources. The manufacturer's website has high level specifications such as SLS thrust, OPR, FPR, BPR, fan diameter, and engine length. The Type Certification Data Sheet[2] (TCDS) gives information such as the number of stages in the compressors and turbines and sometimes gives speed limits for the low and high pressure spools. The most important public information available for performance matching comes from the ICAO Aircraft Engine Emissions Database[1] which gives SLS fuel flow and emissions data for the four ICAO modes (100%, 85%, 30%, and 7% of max thrust). The final information which is publicly available is a diagram of the engine flow path, often found in books such as Jane's Aero-Engines [13]. The component lengths, hub dimensions, and tip dimensions can all be calculated from a flowpath diagram and provide vital information for sizing the components correctly. Due to the complex nature of the EDS framework, one does not create a new engine model from scratch. For example, the PW4090 model is based on a model of the GE90. Although these engines differ in performance, the flexibility of EDS allows for conversion of the GE90 model to perform as a PW4090 because they are both high bypass ratio turbojet engines.

Table 3.1: PW4090 Public Data Parameters to Match

Parameter	Value	Units	Parameter	Value	Units
OPR	39.16		BPR	1.6	
Rated Thrust	88800	lb	Turbine Exhaust at TO	1707	R
Fan Stages	1		LPC Stages	6	
HPC Stages	11		HPT Stages	2	
LPT Stages	7		Dry Weight	15741	lb
Fan Diameter	112	in	Length	190.42	in
Fuel Flow			NO_x		
100% Thrust	30936.7	lbm/hr	100% Thrust	61	g/kg
85% Thrust	23627.1	lbm/hr	85% Thrust	42.8	g/kg
30% Thrust	7595.3	lbm/hr	30% Thrust	13.19	g/kg
7% Thrust	2127.0	lbm/hr	7% Thrust	4.29	g/kg

The first step in creating a new engine model is to input all the publicly available specifications, as shown in Table 3.1 for the PW4090. Next, the turbine inlet temperature is varied to match the 100% thrust rating. After this, the pressure ratio split between the LPC and HPC is varied to match the ICAO takeoff fuel flow. The LPT and HPT cooling flows are then changed to match fuel flow at the 85%, 30%, and 7% thrust levels. The HPT cooling flows tend to change the slope of the power hook (a plot of engine thrust versus fuel flow) at 30% and 85% thrust ratings and changing the LPT cooling flows change the power hook most at 50% and 30% thrust. The engine bypass ratio is set by varying the jet exit velocity ratio. Iterating on these first steps allows one to match the model power hook with the ICAO data as shown in Figure 3-1.

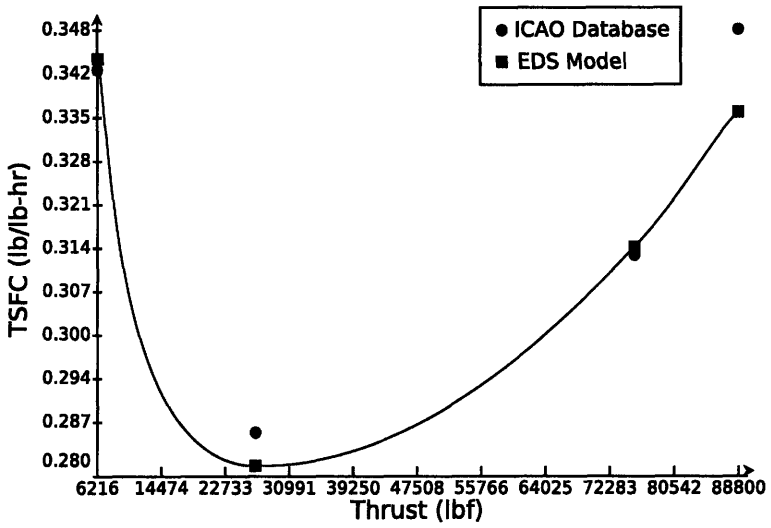

Figure 3-1: PW4090 Power Hook

Once the power hook is matched, the engine component sizes and weights are matched. The fan diameter is matched by changing its hub to tip ratio. The length of the fan is input directly. The number of compressor and turbine stages is varied by changing the first stage pressure ratio limit and blade load factor for each component. The length for each stage is input directly, which along with the lengths input for all the connecting ducts sets the length of the engine. Each component also has a hub to tip ratio input which impacts the cross-sectional area of the core and bypass flow

paths. If the weights computed for the given component lengths are incorrect, weight scale factors can be applied to individual components to correct for any errors. Since the variables changing here are not necessarily independent of the thermodynamic cycle, the process is repeated until the calculated performance matches the available data.

After the engine weight is established, the engine model is flown on an aircraft. The aircraft thrust to weight is varied to get the correct gross takeoff weight for the specified engine. This process is iterative since changes in engine size will cause the aircraft weight to change which will change the amount of fuel required for the mission.

Unfortunately, this process of creating a baseline engine model requires a significant amount of human input and is quite time intensive. In an effort to automate the task, and to remove human prejudices on the baselining process, a method to create baseline models is being developed at the Georgia Institute of Technology which uses a design of experiments and optimization to match the publicly available data with minimal human intervention.

3.4.1 Three Point Design

EDS is setup to perform all the engine design work at SLS conditions, this is called a single point engine design. This is in contrast to the PW design philosophy of using a three point design method incorporating engine requirements at takeoff and top of climb in addition to sea-level static. Due to this difference, future versions of EDS will incorporate a three point design philosophy. In the mean time, an interim three point design method was implemented to aid the comparison between the EDS and PW models. This provided an ability to assess if the differences between the EDS and PW results are due to design point philosophy implemented or if other differences in how the design tools are used cause major differences in the results.

The three point design implemented for this study enforces constraints at top of climb, sea level static, and takeoff. The main engine sizing design point is top of climb, which is where the engine pressure ratios are defined. The thrust is then

defined at SLS and T4 max is defined at takeoff. In addition to these design points, a number of design parameters are met at each design point as noted below.

- TOC thrust = 19000 lb (attained by changing TOC airflow)
- SLS thrust = 88800 lb (attained by changing TOC T4)
- TO T4 (attained by changing SLS T4)
- SLS LP RPM = 2465 (attained by changing TOC LP shaft rotational speed)
- SLS fan design corrected speed = 0.975 (attained by changing TOC fan design point corrected speed)

3.5 Comparisons

3.5.1 EDS vs PW

This section provides a brief overview of the final results from the industry study. Since EDS is used for evaluating policy scenarios, accuracy in trends in more important than matching exact results and because of this all the results are displayed as a relative to the baseline reference case. The plots of mission fuel use, engine weight, and LTO-NO_x emissions are shown as changes from the baseline, by subtracting the baseline value for each point. The plots of TSFC are shown as a percent change from the baseline value. Three plots are shown for each of the outputs including a plot of the EDS results followed by a plot of the PW results and a plot of the percent error of the EDS results when compared to the PW results.

As shown in Figure 3-2(a), the range of TSFC over the entire design space for the EDS results is about twice as large the range in the PW results. The shape of the trend lines are similar when T4 is increased above the baseline value, but the PW results display non-linear effects when T4 is decreased. This may be due to changes in component efficiency and cooling flow which are not currently modeled in EDS. This effect, which occurs in a real engine, would cause the EDS trends to show more of a curve as the PW results shows. The bucket in this curve represents an optimal design T4 for a given OPR and is even more apparent in the block fuel plot show

in Figure 3-2(b). The discontinuity in the EDS results is due to a change in engine weight which propagates through to the mission fuel use. The change in engine weight is due to an increase in the number of LPT stages.

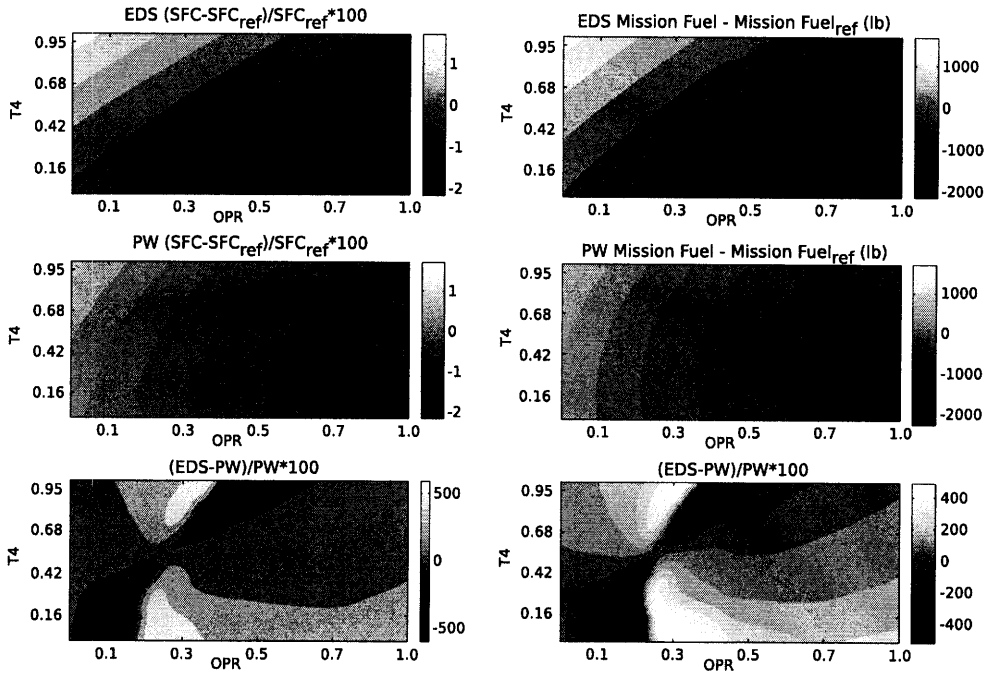

(a) TSFC

(b) Mission Fuel Burn

Figure 3-2: EDS vs PW: TSFC and Mission Fuel Burn

Similar to TSFC, the range of engine weight over the design space for the EDS results is about twice as large as that shown in the PW results. The trends between the two sets of results are very similar. They exhibit significant changes in engine weight as T4 changes, but minimal changes with OPR. The one exception is at the discontinuity in the EDS results. At this pressure ratio, the algorithm in WATE determines that an additional LPT stage is required. The weight of that additional stage is what causes the abrupt increase in engine weight.

Since both EDS and PW use simplified empirically based models for emissions, the results match well as expected. The differences in the results are most likely due to differences in the emissions models. There may also be variation due to burner entrance pressure and temperature computed by EDS. This difference can be attributed to variation in the method used for the three point design and the specifics

of what TOC thrust is required.

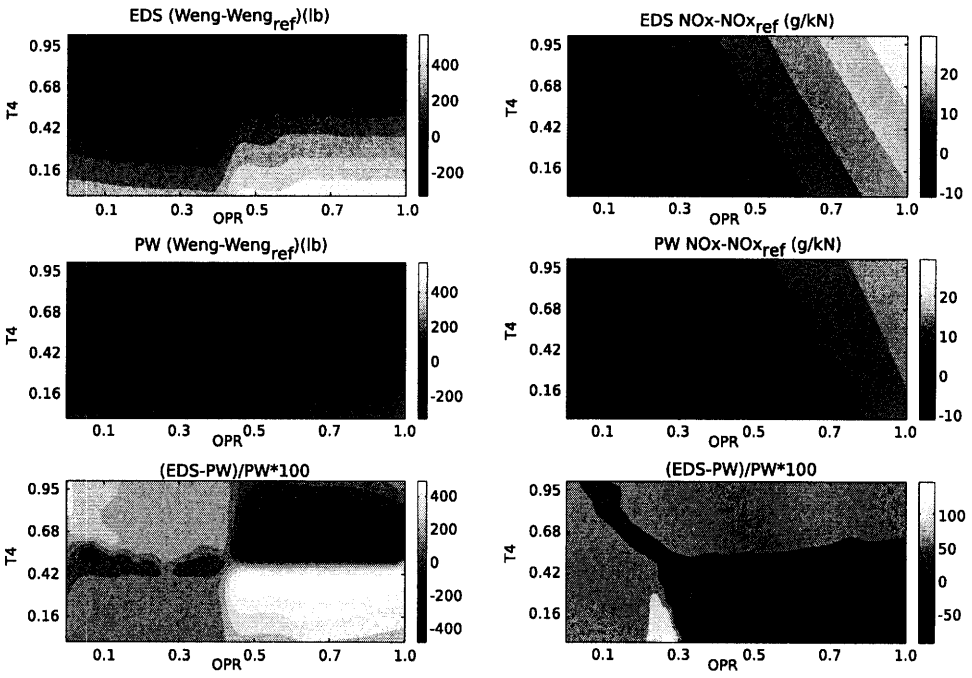

(a) Bare Engine Weight

(b) LTO-NO_x

Figure 3-3: EDS vs PW: Engine Weight and Emissions

3.5.2 Single Point vs Three Point Design

This first round study with Pratt & Whitney was designed to evaluate EDS's overall design method. As an example of the developments in EDS due to the study, this section compares results from EDS before and after the three point design method was implemented. As shown in Figure 3-4, the TSFC trends changed significantly. Both the direction and scale of the trend changed.

The engine weight, shown in Figure 3-5, indicates another important difference between the single and three point design methods. In the single point design method, the number of LPT stages increases at two overall pressure ratios, while in the three point design method, the engine weight only increases in one place due to an increase in the number of LPT stages. The three point design method only increases the number of LPT stages once because there is a smaller increase in LPT pressure ratio

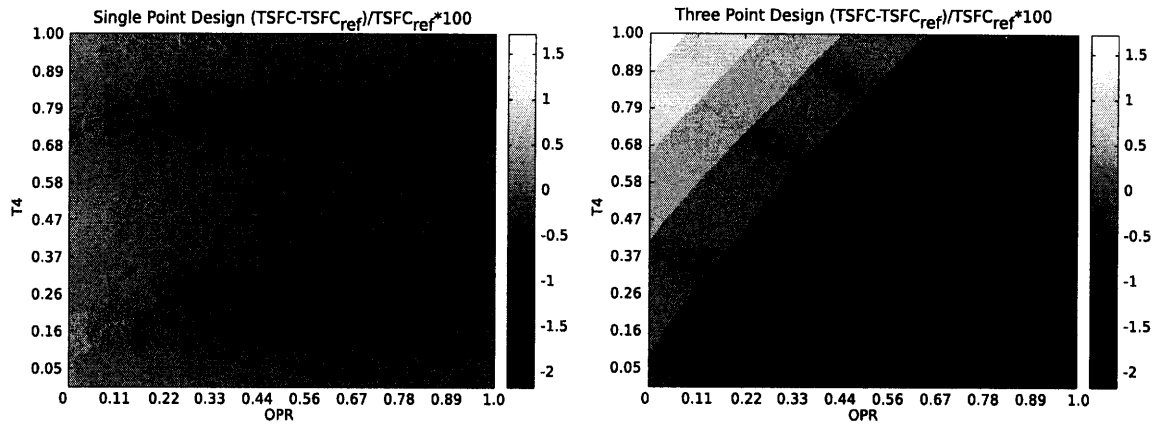

(a) Single Point Design

(b) Three Point Design

Figure 3-4: Single vs Three Point Design: TSFC

which is caused by limiting the low pressure spool speed.

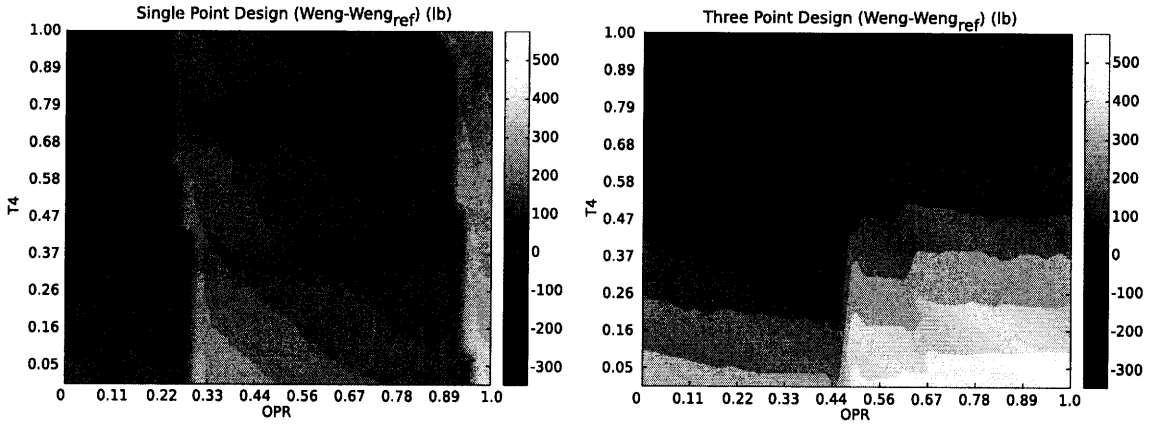

(a) Single Point Design

(b) Three Point Design

Figure 3-5: Single vs Three Point Design: Bare Engine Weight

The range of LTO-NO_x emissions did not change significantly between the single and three point design methods. This is because LTO-NO_x emissions are dependent on the temperature and pressure in the engine when run at SLS conditions. For the single point design method, these are used as an input for the study. The shift in trend direction for the three point design method is because this method uses the input OPR at top of climb and the input T4 max is used at takeoff. EDS then calculates what the SLS conditions are.

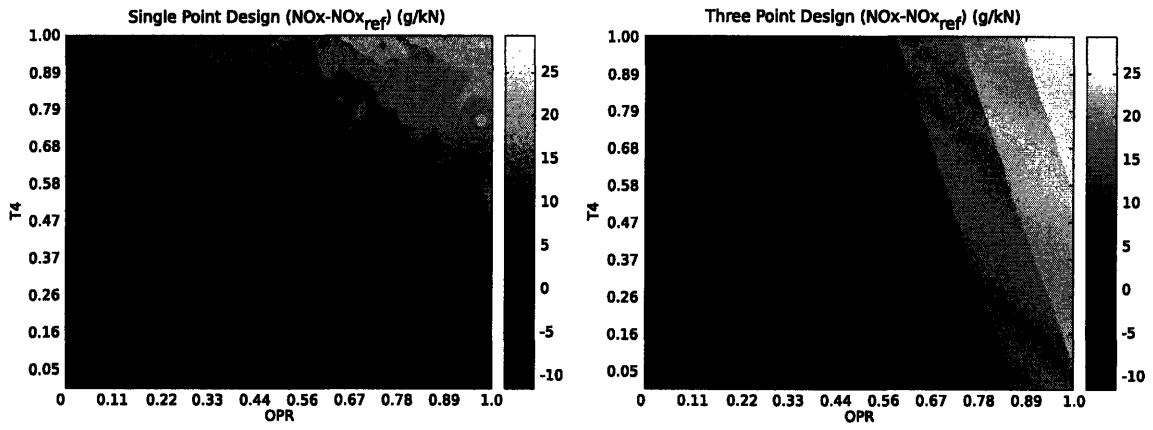

(a) Single Point Design

(b) Three Point Design

Figure 3-6: Single vs Three Point Design: LTO-NO_x

Another thing to note is that the three point design method produced significantly smoother results than the single point design method because of the convergence cycle added to meet the new performance constraints. This is obvious in the LTO-NO_x emissions shown in Figure 3-6, but is apparent in all the results from the single point design method.

3.6 Conclusions

As noted in Section 3.4.1 the major discrepancy between the EDS and PW design methods is that PW uses a three point engine design. This result was also found during the industry study with GEAE which indicates that using a three point design is likely a common industry practice. While this study showed that switching to a three point design method will improve EDS design accuracy, there is a significant amount of development that remains to be done on the EDS three point design method.

A final observation from this study, although not specifically related to the PW results, is that the current method of creating baseline engines models is flawed. The process relies too heavily on human intervention and suggestion allowing the engine design experience of any given person to dictate the design. This can prevent the

baseline from predicting the public data by a significant amount. As an example, the initial model for this study was limited to having a turbine inlet temperature of 2900 R based on experience with other engine models. This caused difficulty in creating a baseline model which matched public data but the limit remained until input from Pratt & Whitney indicated the need for a higher turbine inlet temperature. The ongoing work at Georgia Tech to create baseline models using a semi-automated design of experiments will resolve this issue.

Chapter 4

Model Assessment

4.1 Introduction

This chapter investigates EDS model sensitivity and uncertainty. The model assessment is broken into five sections starting with a sensitivity study on the model inputs. The second study considers sensitivities of the compressor component map. The third study addresses the constraints implemented during EDS runs and an example problem of implementing additional constraints on EDS results. Model uncertainty is assessed using Monte Carlo simulations which vary all the model inputs. Finally, the ability of EDS to calculate higher confidence results than system level uncertainty would allow for is quantified.

4.2 Motivation

In addition to validating design tools with public data it is important to investigate the effect of changing the inputs and constraints implemented in the design tools. Due to the complex nature of multidisciplinary design tools, such as EDS, the effect of changing inputs is not necessarily what one would expect. These effects are investigated using sensitivity studies on both the inputs and constraints.

The uncertainty of a design tool is also important when considering trade studies produced. Uncertainty in EDS stems from two sources - uncertainty due to the

computational methods used in the model and uncertainty due to lack of knowledge of the inputs. The first type of uncertainty is often caused by approximations in the design tool solution methods. Uncertainty due to lack of knowledge of the inputs is investigated using Monte Carlo simulations.

4.3 Sensitivity Study

4.3.1 Input Variable Categorization

The EDS input variables are split into four groups, shown in Table 4.1, based on the impact they have on fuel burn, noise, and emissions calculated using a decoupled sensitivity study. The effect, ε, of the input variable is defined as the percent change in the output of interest divided by percent change in the input variable. This nondimentionalizes all the inputs in a consistent way to determine which of them has the most effect on the output. The most important inputs, defined as major drivers, are those that affect the output most significantly and special care must be given when picking the uncertainty distributions for the Monte Carlo simulations.

Table 4.1: Input Variable Categorization

Categorization	Effect
Major Driver	$\varepsilon > 0.1$
Minor Driver	$0.1 \geq \varepsilon > 0.005$
Insignificant	$0.005 \geq \varepsilon > 0$
No Effect	$\varepsilon = 0$

No effect variables often have no effect because they are variables that are required to be in the input files for EDS to run but are not used based on how the solver is setup. For example, EDS requires that both design thrust and design airflow are in the input file. When the model is created, design thrust is set as a dependent variable with airflow as its independent variable. In this mode, airflow is scaled to give the desired thrust value. Once the engine model is calibrated, this relation is turned off and airflow becomes a dependent variable with thrust as its variable. This renders

the design thrust value in the input file inconsequential during any further use of the model.

4.3.2 Output Variable Evaluation

EDS calculates hundreds of performance parameters for every aircraft analyzed but many of these performance parameters are insignificant when put into the context of APMT. The most important outputs from EDS are fuel use, LTO-NO_x, and aircraft noise. Fuel use is computed by FLOPS as the fuel burned by the aircraft to fly a given mission. In the case of this study, a mission of 3000 nmi was used, which represents a standard flight for the Boeing 777-200. Fuel burn proves to be a useful output not only because it directly impacts operating cost, but it is also an indicator of both aircraft and engine performance as shown in the Bregeut range equation,

$$R = \frac{V(L/D)}{g \cdot TSFC} ln\left(\frac{W_i}{W_f}\right)$$

where R is range, V is aircraft velocity, g is acceleration due to gravity, $TSFC$ is thrust specific fuel consumption, L/D is the lift to drag ratio, W_i is the initial aircraft weight, and W_f is the final aircraft weight. In the case of constant range, the fuel used will change based on changes in aircraft and engine performance. This is balanced by changing the weight of fuel carried on the mission, which directly impacts the initial and final aircraft weight in the equation above.

The total aircraft emissions are represented by the landing-takeoff cycle emissions. Although an aircraft engine creates emissions throughout the entire flight, the emissions generated while the aircraft is below 3000 ft are the most regulated. Because it is the most highly regulated condition, most of the current empirical data and prediction methods focus on emissions created near sea level conditions. In fact, the standard ICAO procedure to certify an engine's emissions is a test conducted at SLS conditions where the engine is run at four throttle settings which are meant to represent the four segments in the LTO cycle.

Aircraft noise is certified by measuring the noise at three locations during the LTO cycle. Federal Aviation Regulation Part 36[3] (FAR 36) defines these points as

shown in Figure 4-1. Landing noise is measured directly under the flight path at the approach point. Takeoff noise is measured both directly under the flight path at the flyover point and to the side at the sideline point. The sideline point is intended to account for noise the community near the airport would experience.

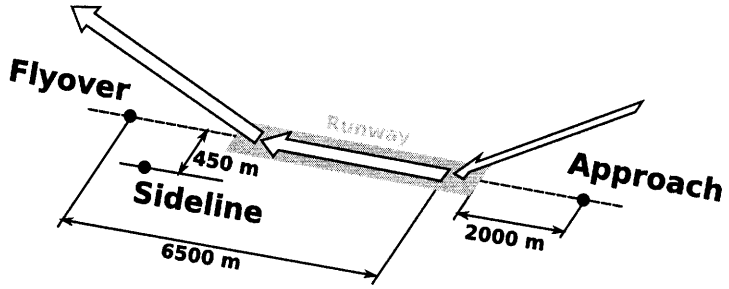

Figure 4-1: FAR 36 Microphone Locations for Aircraft Noise Measurement

The metric used to summarize aircraft noise for this thesis is the cumulative effective perceived noise level (EPNL) which is the sum of the EPNL measurements at the three FAR 36 locations. The EPNL at each location weights frequencies which are most annoying to the human ear and accounts for the duration of exposure.

4.3.3 Decoupled Sensitivity Study Method

A decoupled sensitivity study is a simplest way to assess the nearly 400 inputs of EDS. The study is performed by systematically increasing and decreasing each of the inputs by 2.5% from the baseline value in 0.5% increments. The study is two sided (ie increase and decrease each input) because there are a number of inputs in which moving one direction or the other does not make physical sense, such as increasing efficiencies above 100%. The results from each run are compared to the results from the baseline case and ranked based on how much they affect the outputs of interest. Although this method provides a simple way to assess the impact of various inputs, information about higher order effects due to variable coupling cannot be extracted from this study. The variables that have no effect on the outputs will be removed from the list of inputs studied for the Monte Carlo simulations.

Table 4.2: Sensitivity Results: Fuel Burn

Input	ε	Input	ε
Total Gross Thrust Loss	-4.90	Fuselage Depth	0.35
Bypass Nozzle Velocity Coef.	-3.30	No. Flight Crew	0.33
Fuel Heating Value	-1.65	No. Coach Passengers	0.33
Burner Efficiency	-1.65	Fuselage Weight Factor	0.28
Design Range	1.55	Wing Weight Factor	0.25
Lift-Independent Drag Coef.	1.01	Airfoil Technology Factor	-0.21
Core Nozzle Velocity Coef.	-0.89	Passenger Weight	0.20
Wing Aspect Ratio	-0.76	Wing Area	-0.20
Cruise Mach Number	0.73	Thrust to Weight Ratio	0.20
Fuselage Length	0.64	Furnishings Weight Factor	0.15
Lift-Dependent Drag Coef.	0.64	Fan Map NcDes	-0.14
Wing Thickness to Chord Ratio	0.50	HPC Map NcDes	-0.11
Fuselage Width	0.37	Horizontal Tail Area	0.11
Number of HPT Stages	-0.35	HPC PR	-0.11

4.3.4 Impact on Fuel Burn

More input variables impact fuel burn than LTO-NO_x or noise. As shown in Table 4.2 there are a total of 29 major drivers for fuel burn, while there are only 14 for LTO-NO_x. This is because fuel burn is impacted by changes to both the engine and the airframe while LTO-NO_x, at least to the first order, is only impacted by changes to the engine. The largest driver for fuel burn is the total gross thrust loss which is a scale factor that is applied to the thrust calculated before it is output from the engine analysis. Although this is the largest driver, it is not of particular interest because it will not be used in practice. It is a tuning factor that can be applied to scale an engine one direction or the other without having to get into the details of changing the engine size, pressure ratio, or temperatures to vary the thrust. The next major driver, bypass nozzle velocity coefficient, is more interesting.

Bypass nozzle velocity coefficient, C_v, is the ratio of estimated nozzle velocity to theoretical exit velocity. This is in effect an efficiency factor for the nozzle. The velocity coefficient is multiplied on the momentum portion of the nozzle thrust equation,

$$T = \frac{W}{32.174} V C_{mixCorr} C_v + (P_s - P_{so}) A \tag{4.1}$$

where W is the mass flow in lb/s, V is the theoretical flow velocity in ft/s, P_s is the flow static pressure in psi, P_{so} is the ambient static pressure in psi, A is the physical cross-sectional area of the nozzle in in^2, and $C_{mixCorr}$ is a thrust correction due to partial mixing upstream or in the nozzle. An effect of -3.30 means that when C_v is decreased by 0.5%, fuel burn will increase by 1.65%. The large effect of C_v is due to the design constraints embedded in the EDS models. EDS is setup such that the thrust to weight ratio of the aircraft is constant, a constraint which is implemented in FLOPS and discussed in detail in Section 4.5.3. Take, for example, the case when bypass nozzle C_v is decreased by 0.5%. NPSS first computes the engine thrust to be 88337 lb (0.5% less than the baseline value). FLOPS uses this engine design and finds that the engine has to be scaled up to 89672 lb thrust to meet the range requirement and to keep the trust to weight ratio constant at 0.26. NPSS recalculates the engine using the scaling factor computed by FLOPS and designs an engine with 89671 lb thrust which FLOPS then finds acceptable to fly the design mission. The net effect is that both thrust and aircraft gross weight are increased by 0.99%. In addition, the thrust specific fuel consumption is increased by 0.3%. These changes compound to create the large effect the bypass nozzle C_v has on fuel burn.

The next two largest major drivers, fuel heating value and burner efficiency, have almost identical impacts on the aircraft. The thrust to weight constraint in FLOPS plays a large role in these variables as well. As an example, decreasing burner efficiency by 0.5% will increase fuel burn by 0.83%. For this case, NPSS first computes the engine at 88795 lb thrust (only 0.006% low) but the thrust specific fuel consumption is 0.338 (0.6% higher than the baseline case). FLOPS again scales the engine up to 89204 lb thrust (a 0.46% increase) to maintain a constant thrust to weight ratio. After NPSS reanalyzes the engine and FLOPS executes another minor scaling, the final engine has a thrust value which is 0.46% higher than the baseline and the thrust specific fuel burn is 0.54% higher. These changes combine to create a 0.83% increase

in fuel burn.

The largest fuel burn driver that is not an engine parameter is the design range. One might initially expect design range to have a one to one relation with fuel burn. It is intuitive to think that it will take half as much fuel to fly half the distance. Again due to the thrust to weight ratio constraint this relation is not one to one, although it is linear. When design range is decreased by 0.5%, FLOPS scales the engine down by 0.42%. The aircraft gross weight also decreases by 0.42% which is due to a smaller, lighter engine and the fact that less fuel is needed for the mission. Since the engine sizing process does not effect the performance of the engine, the thrust specific fuel consumption remains at the baseline value. The large decrease in fuel burn of 0.77% is because both the range and the initial weight of the aircraft were decreased.

4.3.5 Impact on LTO-NO_x Emissions

The largest LTO-NO_x driver, as shown in Table 4.3, is the fan pressure ratio (FPR). Decreasing FPR by 0.5% decreases LTO-NO_x by 1.3%. The initial engine analysis in NPSS creates a 88248 lb thrust engine. FLOPS scales this up to 88813 lb to be able to fly the mission. This creates an engine that has lower internal pressure and temperature when compared to the baseline case but is physically larger and thus able to produce the required amount of thrust. Since both P_{T3} and T_{T3} (the pressure and temperature at the high pressure compressor exit) are lower, the emissions indices computed at all thrust levels are lower by up to 0.89%. The lower emissions indices and 0.48% lower thrust specific fuel consumption (due to the lower FPR) combine to decrease the LTO-NO_x by 1.3%.

The next two largest major drivers, the low and high pressure compressor pressure ratios, have impacts which work in similar ways. Like decreasing FPR, decreasing LPC PR or HPC PR leads to lower pressures and temperatures in the engine. This decreases the emissions indices just like decreasing FPR does. Unlike decreasing FPR, decreasing LPC PR or HPC PR increases the thrust specific fuel consumption (making the engine less fuel efficient). When computing LTO-NO_x, this offsets part of the decrease in the emissions indices and leads to an overall lower, but still significant

Table 4.3: Sensitivity Results: NO_x

Input	ε	Input	ε
Fan PR	2.61	HPC Map NcDes	-0.34
LPC PR	1.56	Core Nozzle Velocity Coef.	-0.33
HPC PR	1.55	Exit Velocity Ratio	0.20
Burner Efficiency	-1.01	Ambient Temperature Delta	0.19
Fuel Heating Value	-1.01	Fan Map NcDes	-0.17
Total Gross Thrust Loss	-0.99	Fan Map Rline	-0.13
Bypass Nozzle Velocity Coef.	-0.65		

effect when compared to FPR.

As discussed earlier, burner efficiency and fuel heating value have very similar impacts through the engine sizing process FLOPS goes through. When burner efficiency is decreased by 0.5%, the final thrust specific fuel consumption is increased by 0.54% and final thrust is increased by 0.46% due to the thrust to weight constraint. The changes in P_{T3} and T_{T3} are two orders of magnitude smaller than the change in burner efficiency and are thus negligible. The effect of these cases, both of which are near -1, is due to the change in fuel burn.

4.3.6 Impact on Noise

Although 68% of the input variables have an impact on aircraft noise, the vast majority of them have a very small effect. Only 3 variables have an effect large enough to be classified as major drivers, as shown in Table 4.4. The variable with the most impact is fan pressure ratio which is expected since the noise due to the fan is one of the largest noise components of the aircraft. Decreasing FPR by 0.5% causes FLOPS to scale the engine up by 0.64%. This causes the fan diameter to increase by 0.3% and the airflow to increase by 0.64%. The core and bypass exit velocities both decrease by 0.54%. All these changes combine to produce a 0.14% decrease in noise which correlates to an effect of 0.30.

The second largest noise driver is wing aspect ratio. Decreasing AR by 0.5% causes the wing reference area to decrease by 0.05% and wing loading to increase by

Table 4.4: Sensitivity Results: Noise

Input	ε
Fan PR	0.30
Wing Aspect Ratio	-0.13
Core Nozzle Velocity Coef.	-0.11

0.21%. The thrust also increases by 0.23% to maintain the design thrust to weight ratio. The changes in the wing aerodynamics cause the airframe noise to increase when AR is decreased.

The final major driver for noise is the core nozzle velocity coefficient. This case encounters another constraint in EDS which causes unexpected results. Changing the core nozzle C_v does not impact the bypass thermodynamics so the bypass exit velocity does not change, this is determined largely by the FPR and the low pressure turbine. EDS uses a constant exit velocity jet ratio to compute the engine bypass ratio. Since the bypass nozzle velocity does not change, the core nozzle velocity cannot change. When the core C_v is decreased by 0.5%, this leads to an increased core pressure ratio since more back pressure is required to produce the same exit velocity with the lower efficiency nozzle. The core pressure ratio increases by 0.47% and the core Mach number increases by 0.48%. When the engine is scaled, the bypass ratio gets decreased by 0.27% and the propulsive efficiency decreases by 0.22%. All these changes combine to cause a 0.06% increase in noise.

4.4 Compressor Map Sensitivity Study

The component maps greatly impact off-design performance for the engine. The compressor maps are generated using CMPGEN, a NASA code dating back to the early 1980's. The CMPGEN input file consists of the design pressure ratio, design corrected flow, design corrected flow per unit area, design point corrected first stage rotor tip speed, design point efficiency, an array of corrected speeds, and an array of Rline values which are location parameters used to define the operating point on the

map. CMPGEN computes the efficiency, pressure ratio, and corrected flow for each of the Rline/corrected speed combinations. Therefore, the width and length of the component map can be increased or decreased by changing the range of Rline and corrected speed values input.

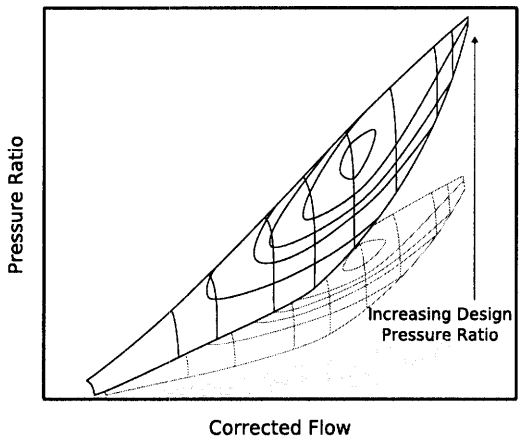

(a) Compressor Map Variation with Design Pressure Ratio

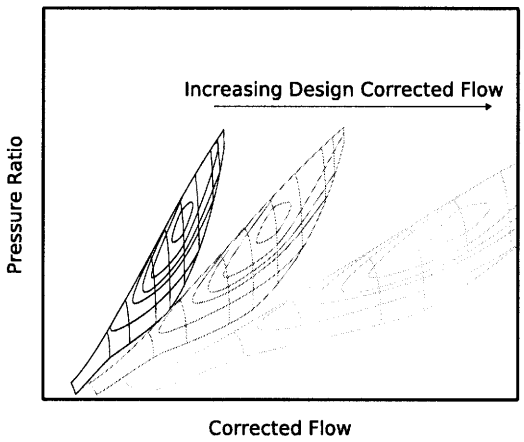

(b) Compressor Map Variation with Design Point Corrected Flow

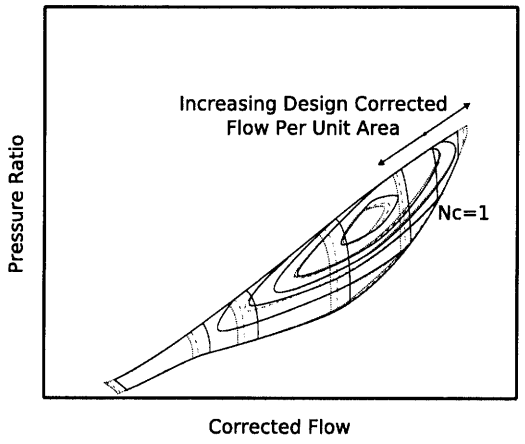

(c) Compressor Map Variation with Design Point Corrected Flow Per Unit Area

Figure 4-2: Compressor Map Sensitivity

Figure 4-2(a) shows how the compressor map changes as the design pressure ratio is changed. As one would expect, as the design pressure ratio is increased the map is stretched vertically so the design point on the map matches the design pressure ratio. In addition to the vertical stretching, the map is also rotated and scaled up on the

horizontal axis.

Figure 4-2(b) shows the impact of changing design point corrected flow on the compressor map. Similar to changing design pressure ratio, the map now stretches match the map design point with the design corrected flow input. This stretching causes the corrected speed lines to become further apart. Along with being stretched, the map is also translated to account for some of the change in design corrected flow.

The third significant input variable, design corrected flow per unit area, expands the corrected speed lines about the corrected speed of one line as shown in Figure 4-2(c). As design corrected speed per unit area is increased, the efficiency islands move with the shifting speed lines. In this case, the range of the map does not change significantly as is did in the previous two cases.

The design point corrected first stage rotor tip speed does not have a significant impact on the shape on the component map. The only impact it has is to make the bottom of the map thinner. Increasing the design point efficiency scales the efficiency lines up such that the efficiency at the design point matches the design point efficiency input.

For preliminary cycle analysis design tools, such as EDS, the detailed characteristics of engine components are not known because the geometry of the component is not defined in detail. This is why it is not possible to perform detailed computation to create custom component maps for each EDS model. It is standard practice to create component maps by scaling some available map. Although NPSS has the ability to scale component maps, the sizing done by CMPGEN is an improved method for representing off design characteristics[6]. For this reason, component maps are generated during the baseline process to minimize the scaling done within NPSS. An important result of this study is that changes in the shape of the component maps due to new technology or differences between engine manufacturers can not be simulated by EDS in detail. In spite of this, the scaling options available in CMPGEN allow the component maps generated for EDS to match the overall performance trends of components in the ranges considered for EDS.

Table 4.5: EDS Constraints

Engine Thermodynamic	Maximum Turbine Inlet Temperature Maximum Fan Corrected Speed Exit Jet Velocity Ratio
Engine Geometry	Bypass Nozzle Location Core Nozzle Exit Area
Aircraft	Minimum Acceptable Climb Rate Thrust to Weight Ratio FAR 25 Takeoff/Landing Requirements

4.5 Constraint Sensitivity Study

EDS has a small number of constraints applied for each case run. EDS takes the approach to not implement constraints in the model but rather to apply constraints to the computed results after a design space has been explored. This limits the number of constraints in EDS to only eight items not including the obligatory constraints such as the engine thermodynamics have to be self consistent and the aircraft has to carry enough fuel to be able to fly the design mission. The constraints are divided into three groups; engine thermodynamic constraints, engine weight constraints, and aircraft constraints as shown in Table 4.5.

4.5.1 Engine Thermodynamic Cycle Constraints

The first thermodynamic constraint, shown in Figure 4-3(a), is the maximum turbine inlet temperature. This limit is a technology factor that gives an indication of the robustness of the turbine material and the cooling technologies implemented. When turbine inlet temperature is increased, the fuel to air ratio must increase the create the higher temperature. Since the bypass duct is unaffected by this, the nozzle exit areas have to change to keep the velocity jet ratio constant (another constraint in EDS discussed below). The increase in turbine inlet temperature leads to a decrease in core nozzle exit area and an increase in bypass nozzle exit area, this is effectively increasing the bypass ratio. The changes in nozzle exit area proportionally impact the thrust generated by each nozzle. Since the core nozzle exit area decreases more

than the bypass nozzle exit area increases, the core nozzle thrust decreases more than the bypass nozzle thrust increases. This leads to a net thrust loss when maximum turbine inlet temperature is increases.

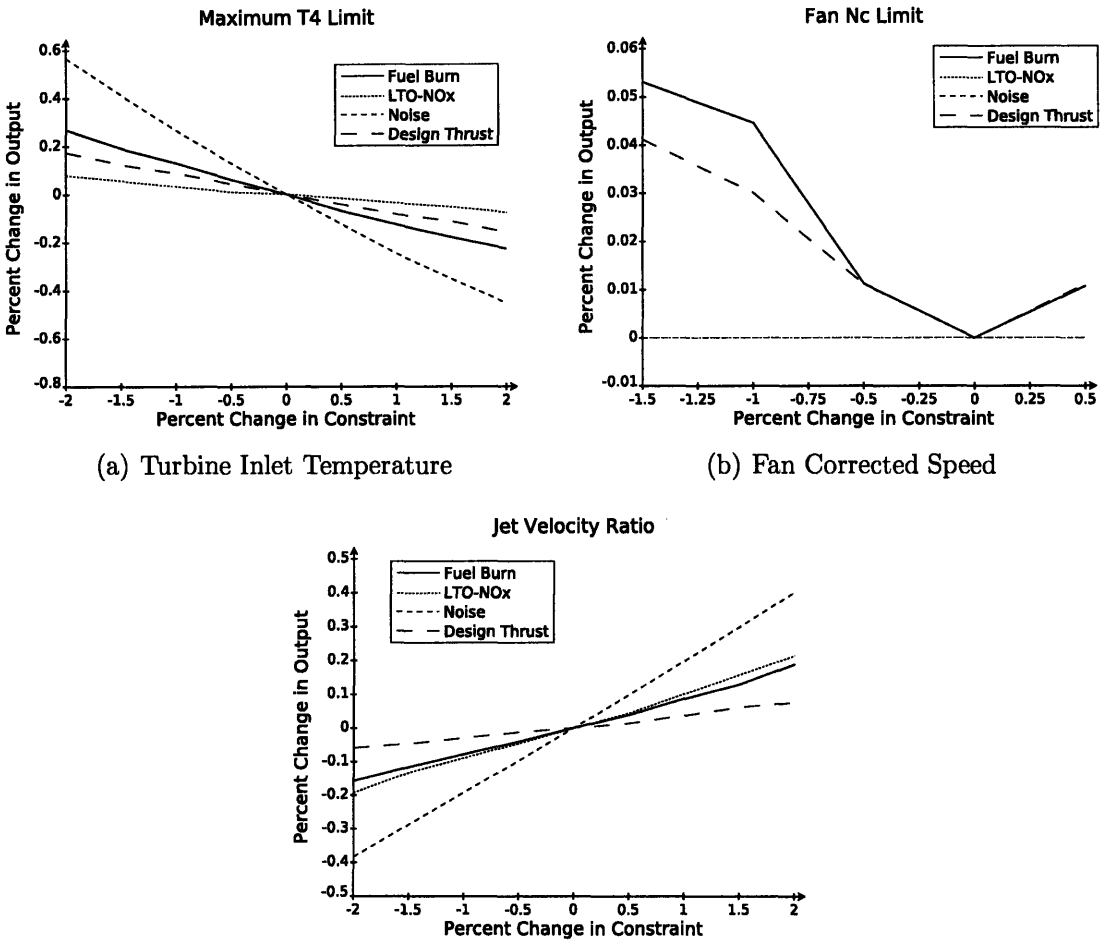

(a) Turbine Inlet Temperature

(b) Fan Corrected Speed

(c) Jet Velocity Ratio

Figure 4-3: Engine Thermodynamic Constraints

The fan corrected speed constraint changes the map scale factor computed by NPSS to match the design point. When the constraint is increased, the map scale factor decreases which decreases the fan corrected flow. Lower corrected flow in the fan propagates through the rest of the engine and leads to lower thrust as shown in Figure 4-3(b).

The constraint on jet velocity ratio impacts the engine design when many of the inputs are varied. This constraint specifies that the ratio of core exit velocity to

bypass exit velocity is constant, a common way to specify the bypass flow relative to core flow. The jet velocity ratio is used for this specification instead of the bypass ratio because the jet velocity ratio has physical ties to the thermodynamics of the engine. In constrast, the thermodynamic implications of changing bypass ratio is less clear. In many cases, such as when changing maximum turbine inlet temperature, the constraint on jet velocity ratio causes the opposite effect as one would expect. When jet velocity ratio is varied on its own the effect of thrust is not as large as expected. As shown in Figure 4-3(c), increasing jet velocity ratio by 2% only increases thrust by about 0.1% when thrust should be increased by 0.5%. This is because FLOPS scales the engine down during the engine sizing loop.

4.5.2 Engine Geometry Constraints

The first engine geometry constraint sets the lengthwise location of the bypass nozzle as a function of the fan diameter. As shown in Figure 4-4(a), increasing the bypass nozzle location constraint moves the bypass nozzle further down the engine. This leads to a longer bypass duct which causes the engine to be heavier. The heavier engine requires FLOPS to scale the engine up during the engine sizing loop which causes the design thrust and fuel burn to increase.

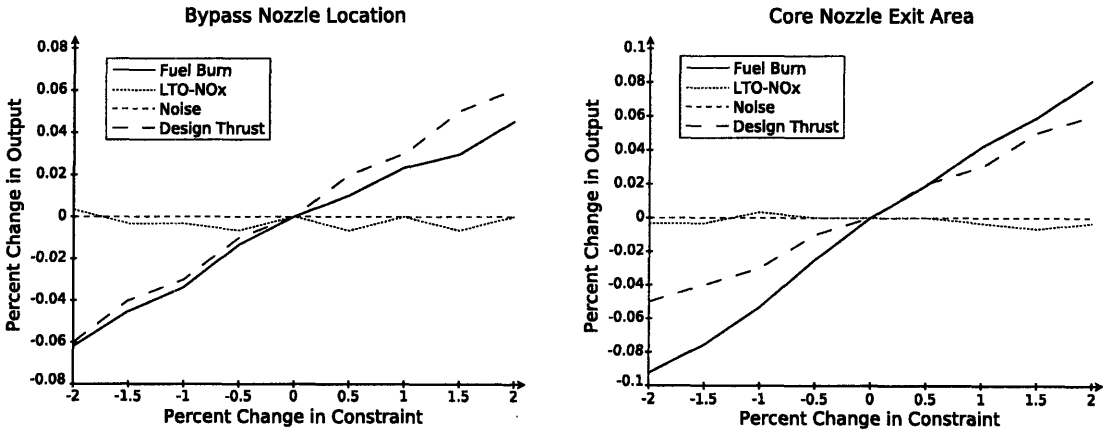

(a) Bypass Nozzle Location

(b) Core Nozzle Exit Area

Figure 4-4: Engine Geometry Constraints

The second engine geometry constraint sets the core nozzle exit area to match 95%

of the LPT exit area. As the constraint is increased, the core nozzle exit area increases which increases engine weight as shown in Figure 4-4(b). The increase in weight causes FLOPS to scale the engine up during the engine sizing loop. This increases the engine thrust and since the thrust specific fuel consumption is unchanged, the mission fuel burn increases as well.

4.5.3 Aircraft Constraints

The first of the three aircraft constraints is the minimum acceptable climb rate. This constraint is set to 300 ft/min but is not active since the calculated rate of climb never approaches the constraint. The only active FLOPS constraint is the aircraft thrust to weight ratio shown in Figure 4-5.

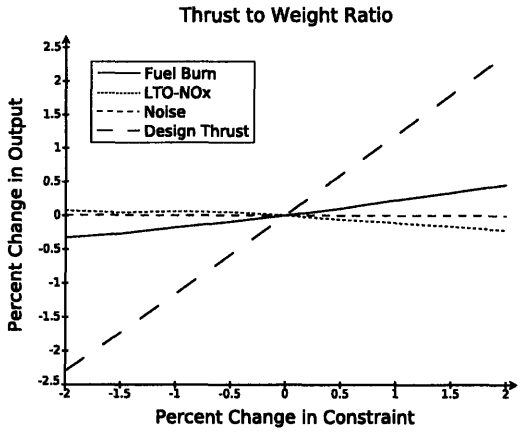

Figure 4-5: Aircraft Thrust to Weight

Scaling the thrust to weight ratio up causes FLOPS to scale the engine thrust up which is done by increasing the engine area. This also increases the engine weight which causes FLOPS to compute a required thrust higher than the increase in thrust to weight ratio would predict. This compensation for increased engine weight is why the design thrust line in Figure 4-5 has a slope higher than one. Since the engine sizing process does not effect the basic thermodynamic cycle of the engine, the thrust specific fuel consumption remains constant even through the design thrust increases. The change in fuel burn is simply caused by the increase in thrust.

Similar to the jet velocity ratio constraint, the thrust to weight constraint is an active constraint and can cause unexpected results. The thrust to weight ratio is the key parameter used during the engine sizing loop which often causes an inverse effect in engine thrust. For example, decreasing fan pressure ratio initially decreases computed thrust, as expected, but FLOPS scales the engine up to maintain a constant thrust to weight ratio. Once the engine sizing loop converges, the engine has more thrust than the baseline case which is a counterintuitive result. Although this constraint can produce unexpected results, it is necessary to maintain aircraft maneuverability especially during take off and climb out.

The final aircraft constraint ensures that the aircraft meets FAR 25[3] takeoff and landing requirements. These constraints are embedded in FLOPS and are applied to every aircraft designed by FLOPS. In fact, the FAR 25 second takeoff segment climb gradient is an active constraint which sizes each aircraft designed by FLOPS. The takeoff and landing module in FLOPS not only checks these constraints but actually applies them during the takeoff and landing profile computations to ensure they are met[23].

4.5.4 Additional Constraint Implementation

In the current incarnation of EDS the design space of an aircraft-engine model is explored using a design of experiments which spans a large range for all the input design variables of interest. The results from this design of experiments are fit using response surfaces[18] to approximate relevant outputs. Constraints are then applied using results from the response surfaces instead of applying constraints on the original results from EDS. This can lead to unnecessary errors such as those in the following example.

The sample design of experiments looks at variation in wing aspect ratio (AR) and aircraft thrust to weight ratio (TWR). These inputs are varied by $\pm 10\%$ in 0.5% increments using a full factorial design of experiments. The constraint applied limits takeoff field length to 12,000 ft (the baseline takeoff field length is 10,800 ft). Figure 4-6 shows the takeoff field length computed by EDS. Intuitively, increasing wing aspect

ratio makes the aircraft more aerodynamically efficient which means less fuel is used so the gross takeoff weight decreases allowing for shorter takeoff field lengths. As thrust to weight ratio is increased, thrust increases quicker than gross weight which also allows for shorter takeoff field lengths.

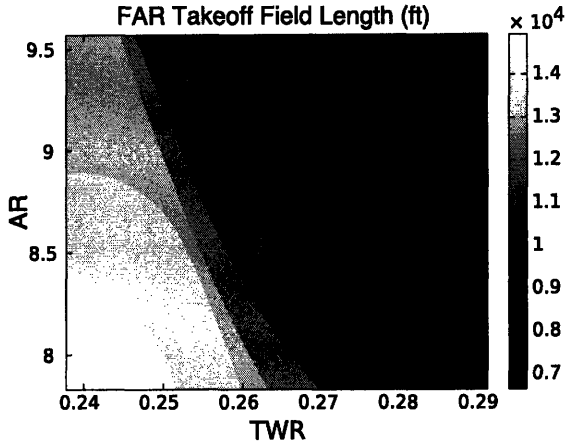

Figure 4-6: FAR 25 Takeoff Field Length

The first case investigated fits a response surface to the results then applies the 12,000 ft field length constraint using results from the response surface. The second case applies the constraint first, on the raw EDS results, then fits a response surface to the down selected results. Second order response surfaces are used for both cases with a least squares minimization[19] (adding third order terms did not produce better surface fits). Figure 4-7 shows the actual versus response surface predicted takeoff field length for both cases. From this plot alone, it is apparent that when the constraint is applied first the points are closer to the diagonal line, indicating a better surface fit. To further this point, R^2 is 0.973 and the root mean square error is 369.41 when the results are fit before the constraint is applied. When the constraint is applied before the response surface is created, R^2 increases to 0.995 and the root mean square error decreases to 86.40.

Figure 4-8 shows the percent error in takeoff field length for both response surfaces and the difference in percent error for the two cases. When the response surface is fit first, there is a large amount of error induced by the very large takeoff field length cases when aspect ratio and thrust to weight ratio are low. When the constraint is

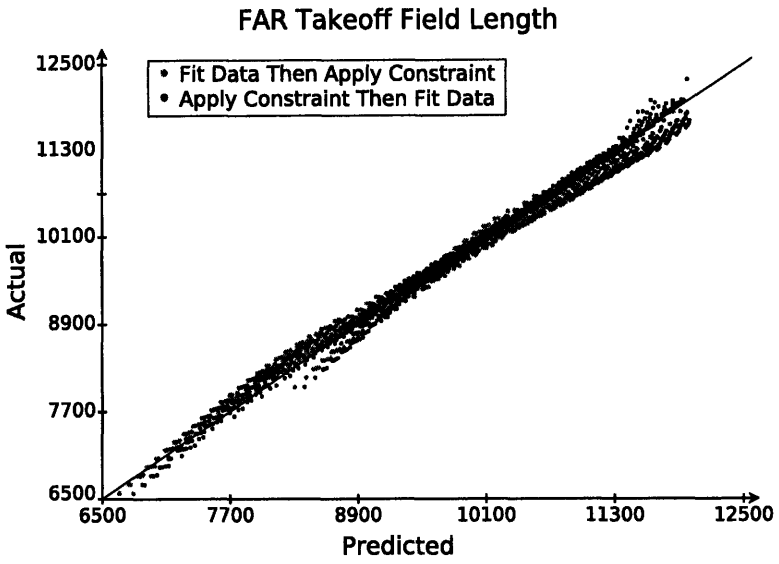

Figure 4-7: Response Surface Residuals

applied before the response surface is created, the overall error decreases. The most substantial difference between the two response surfaces is the difference in slope caused by including the high takeoff field length cases as indicated by the difference in percent error plot. The discontinuity near aspect ratio of 8.7 is caused by a shift in the aborted takeoff field length. This shift is caused by a change in the decision point when the engine thrust reversers are engaged.

For this sample case, the differences in response surfaces cause a difference in an optimal aircraft in terms of fuel burn. Since fuel burn decreases with increasing aspect ratio and decreasing thrust to weight ratio, the optimal aircraft is at the top left of the feasible design space. In all cases, this is a point where the takeoff field length is an active constraint. Using the raw EDS results, the optimal aircraft has an aspect ratio of 9.57 and a thrust to weight ratio of 0.2465 with a mission fuel burn of 273,300 lb. The optimal aircraft using the response surfaces are outlined in Table 4.6.

When the constraint is applied first, the takeoff field length is under predicted by 2.15% in the region where fuel burn is minimized. This causes lower values of thrust to weight ratio to still meet the constraint so a lower thrust to weight value is computed as the optimal value. When the response surface is fit first, it fits the EDS results better in the region where fuel burn is optimized which causes the optimal

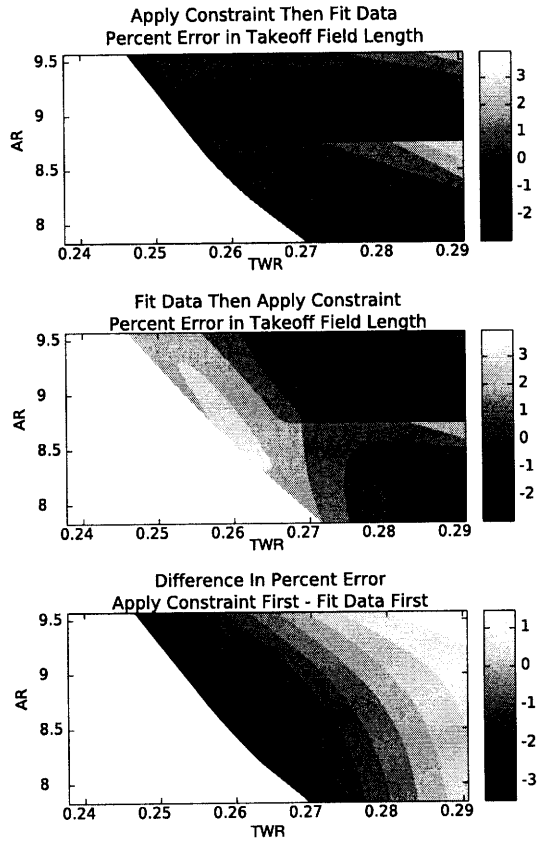

Figure 4-8: Response Surface Comparison

Table 4.6: Constraint Implementation Optimal Aircraft

	TWR	AR	Mission Fuel Burn (lb)
EDS Data	0.2465	9.57	273,300
Fit Data First	0.2458	9.57	273,200
Apply Constraint First	0.2432	9.57	272,800

value to be closer to real optimal value found by using EDS results.

As shown with this simplified example, fitting response surfaces to results before constraints are applied can cause substantial error. In this example, the areas of largest non-linearity were on the infeasible side of the constraint which is why the response surface fit better when this region was disregarded. Although this will not always be the case, constraints can affect design decisions a great deal and care is needed in handling them when creating response surfaces.

4.6 Monte Carlo Simulations

4.6.1 Input Distributions

To maintain consistency throughout the Monte Carlo simulations discussed in this thesis, and with studies performed with the rest of the EDS project, the same uncertainty distribution function should be used on all the input variables. Since there are distribution shapes required for various input parameters something as simple as the normal distribution would not provide adequate flexibility. The beta distribution, on the other hand, includes two shape factors which allow for large flexibility in the shape of the distribution. The probability density function of the beta distribution is given by,

$$f(x;\alpha,\beta) = \frac{1}{\int_0^1 t^{\alpha-1}(1-t)^{\beta-1}dt} x^{\alpha-1}(1-x)^{\beta-1}$$

where the shape factors α and β must be positive[4]. The shape factors provide the ability to represent a wide range of uncertainty distributions from one representing the normal distribution to one-sided distributions. Figure 4-9 shows the shapes of distributions used in this thesis.

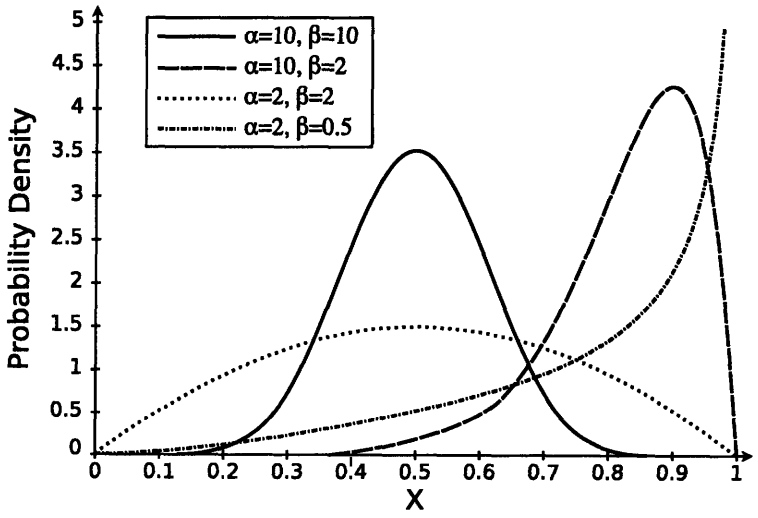

Figure 4-9: Beta Probability Density Function

A beta distribution with $\alpha = \beta = 10$ is ideal for the vast majority of the input variables, but there are some, such as component efficiencies and maximum temperatures which do not physically lend themselves to a symmetric distribution. For these inputs, a more one sided function, such as $\alpha = 10, \beta = 2$, was used. In extreme cases, such as the core nozzle C_v, where the baseline value is very near the physical limit a highly one sided function, such as $\alpha = 2, \beta = 0.5$, was used to prevent moving beyond what is physically reasonable.

Since the uncertainty on the inputs represents an uncertainty in knowledge, the inputs are assumed to be independent. The inputs are sampled randomly and separate from one another for the Monte Carlo simulations. The majority of the inputs have a range of $\pm$ 1.5% of the baseline value. Some inputs, such as component efficiencies, have smaller uncertainties to best approximate the lack of knowledge in the model inputs as shown in Appendix A.

4.6.2 Convergence

Convergence of Monte Carlo simulations is determined by evaluating the mean and standard deviation since there is no residual to reduce as in other types of computational tools. As the number of iterations approaches infinity, the mean and standard deviation of the Monte Carlo sampling will approach their true values. After every iteration, the mean and standard deviation approximate their true values with some confidence band. Once this confidence band is sufficiently small, the Monte Carlo simulation is considered to be converged. The mean and standard deviation are defined as,

$$\overline{x} = \frac{1}{n}\sum_{i=1}^{n} x_i \tag{4.2}$$

$$s = \sqrt{\frac{1}{n-1}\sum_{i=1}^{n}(x_i - \overline{x})^2} \tag{4.3}$$

where $\overline{x}$ is the mean, s is the standard deviation, and n is the sample size. The

confidence intervals for the mean and standard deviation are given by,

$$\langle \mu \rangle = \overline{x} \pm t_{(\alpha/2,n-1)} \frac{s}{\sqrt{n}} \tag{4.4}$$

$$\langle \sigma \rangle = \left[s\sqrt{\frac{n-1}{\chi^2_{(1-\frac{\alpha}{2}|n-1)}}}; s\sqrt{\frac{n-1}{\chi^2_{(\frac{\alpha}{2}|n-1)}}} \right] \tag{4.5}$$

where α is the desired confidence level, $t_{(...)}$ is the upper critical values of the Student's t-distribution with n-1 degrees of freedom, and $\chi^2_{(...)}$ is the inverse of the chi-square distribution with n-1 degrees of freedom[4].

4.6.3 Vary All Uncertainty

The vary all uncertainty study applies uncertainty distributions with a ±1.5% range to all 400 input variables in EDS. This study shows the worst case scenario uncertainty on the EDS results. The uncertainty in the input represents a lack of knowledge in the true value of the input variable. For example, the baseline maximum turbine inlet temperature is 3300 R which is arrived at by attempting to match a thrust level during the baselining process. Since turbine inlet temperature is closely guarded proprietary information, the true value is unknown so an uncertainty distribution is assigned to compensate for this lack of knowledge.

The fuel burn iteration history, shown in Figure 4-10 with a 95% confidence interval, indicates that 1000 cases is more than sufficient to consider the Monte Carlo simulation to be converged. The convergence histories for noise and emissions converge at the same rate as fuel burn.

The uncertainty distributions for fuel burn, LTO-NO_x, and noise are shown in Figure 4-11. The output distributions show an asymmetry favoring the cases with degraded performance. This is especially obvious in the fuel burn and LTO-NO_x distributions as a skew to higher values. This asymmetry in the output causes a shift in the mean value from the baseline case as shown in Table 4.7.

The shift in output is caused by failed EDS runs. NPSS is more likely to be

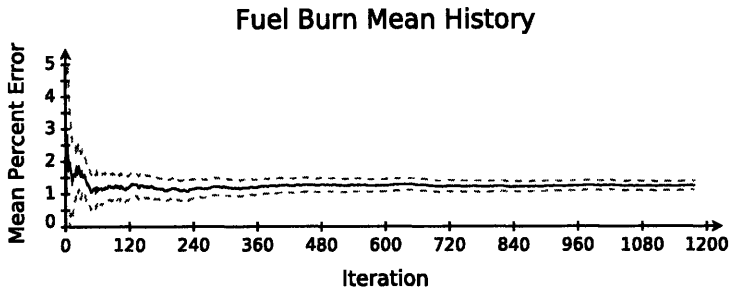

(a) Mean History

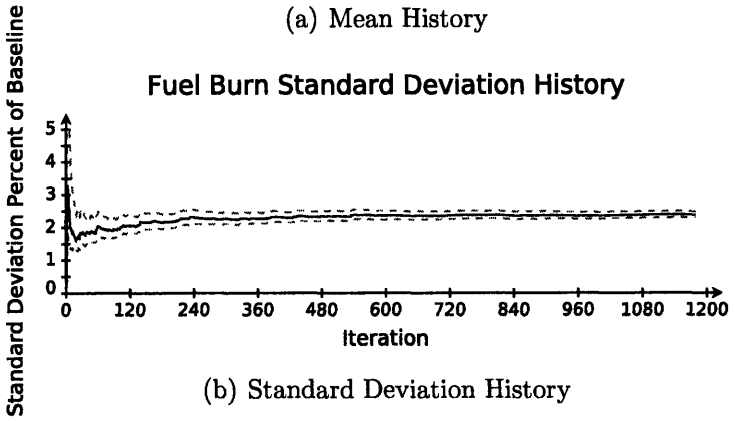

(b) Standard Deviation History

Figure 4-10: Monte Carlo Convergence History

unable to converge on the engine cycle when performance is increased since these are generally more strenuous conditions including higher pressures and temperatures. This leads to the apparent input distributions (being the cases which ran successfully) to be unbalanced. The heavily unbalanced input distributions include major drivers such as the airfoil technology factor, wing aspect ratio, fuel heating value, engine component efficiencies, maximum turbine inlet temperature, and jet velocity ratio.

Table 4.7: Vary All Monte Carlo Results

	Mean Shift from Baseline Value	Standard Deviation (% Baseline Value)
Fuel Burn	2.89%	2.43%
Noise	-0.04%	0.19%
LTO-NO_x	3.47%	2.73%

The number of failed cases is highly dependent on the fan map Rline fix shown in Figure 2-2. With this fix enabled (as in this study) approximately 17% of the cases failed. Without the fan fix enabled, nearly half the cases fail because the operating

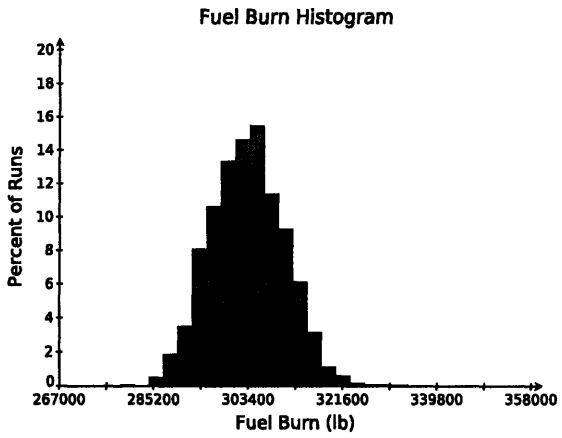

(a) Fuel Burn

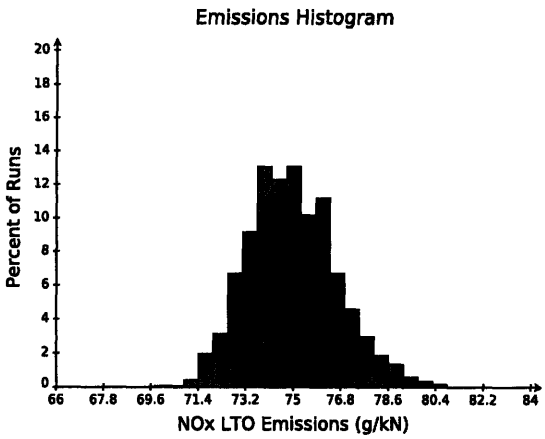

(b) NO_x

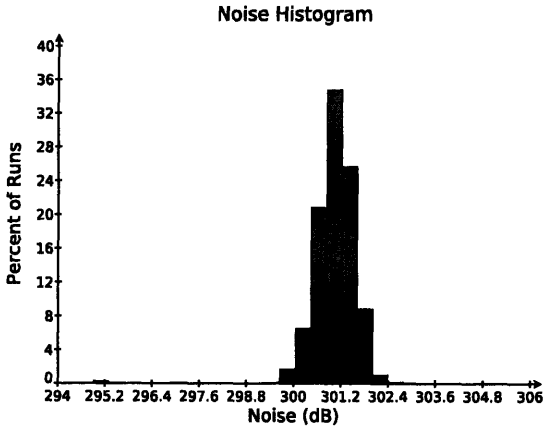

(c) Noise

Figure 4-11: Vary All Uncertainty Results

point is past the stall limit of the component map as shown in Figure 4-12. When the Fan Map Rline fix is enabled, the operating point for the failed case is moved on the map so it runs successfully. Although more cases run successfully with the fan fix enabled, it does not make physical sense to arbitrarily change the component efficiency, pressure ratio, and corrected flow by changing the operating point on the map. The light gray regions on the map show the operating ranges with the fan map Rline fix enabled and the dark gray spots show the operating ranges when the fan map fix is disabled. The systematic decrease in fan Rline to prevent run errors causes an unexpected change in performance which contributes to engine performance uncertainty.

Changing the location on the component map during the flight of a single mission implies there is a variable geometry compressor, which is beyond the technology of interest for this study. If the component map is not wide enough to represent the modeled compressor, the map choke limit can be changed by varying the lower Rline limit input to CMPGEN during component map generation. The map stall limit can be changed by varying the higher Rline limit input to CMPGEN during component map generation. If the operating point goes off the edge of the map the compressor is stalled or choked and the case should fail instead of moving the operating point back onto the map.

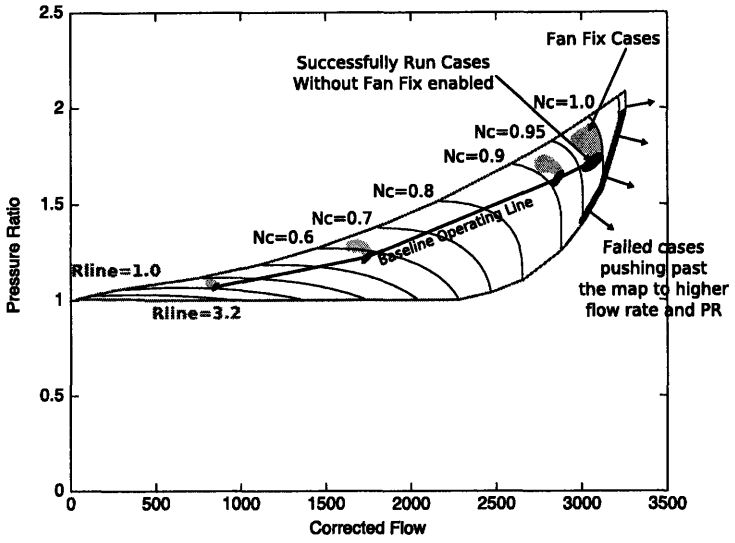

Figure 4-12: Fan Component Map

Although more cases fail when the fan fix is disabled, it gives a more accurate results with lower uncertainties. When the fan fix is disabled, the fuel burn mean shift is decreased by 0.12% and the LTO-NO_x mean shift is decreased by 0.88%. Although these numbers seems insignificant, they are for the case when the input distributions are varied by only $\pm 1.5\%$. When larger variations are applied to the inputs for other studies, the error due to the fan fix will increase.

4.6.4 Sensitivity Study Uncertainty

As shown in Section 4.6.3, the standard deviation for a given design in EDS can be as large as 2.7% for only a ±1.5% variation in the input. This standard deviation is large enough to mask the results from sensitivity studies with small input variation. This section uses an example LPCPR/T4 sensitivity study to show the decrease in standard deviation when comparing two points instead of looking at a single point as done in previous sections. Four points in the design space were investigated; a baseline point, a point for which LPC pressure ratio was changed, a point for which T4 was changed, and a point with both LPC pressure ratio and T4 changed. The LPC pressure ratio is changed by increasing it from 2.4225 to 2.7319 and T4 was changed by increasing from 3300 to 3400 R.

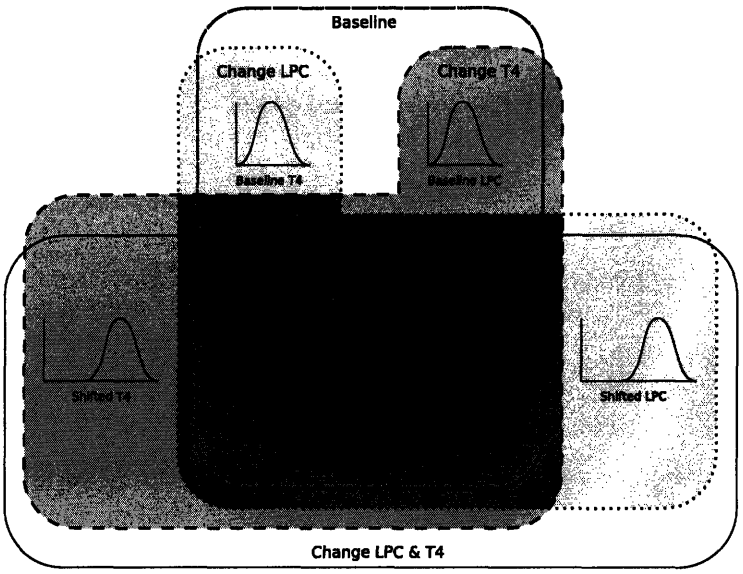

Figure 4-13: Sensitivity Study Uncertainty Input - Four Input Distribution Combinations Indicated by Four Different Line Types

Uncertainty distributions are assigned to all the input variables for the four cases. As shown in Figure 4-13, the baseline case has uncertainty distributions on all the input variables. For the shifted LPC case, a new uncertainty distribution is created for LPC and all the other distributions remain the same as in the baseline case. The same happens for the shifted T4 case. The final case in which both LPC and T4 are

changed uses the shifted uncertainties for LPC and T4 and the baseline uncertainties for all the other variables.

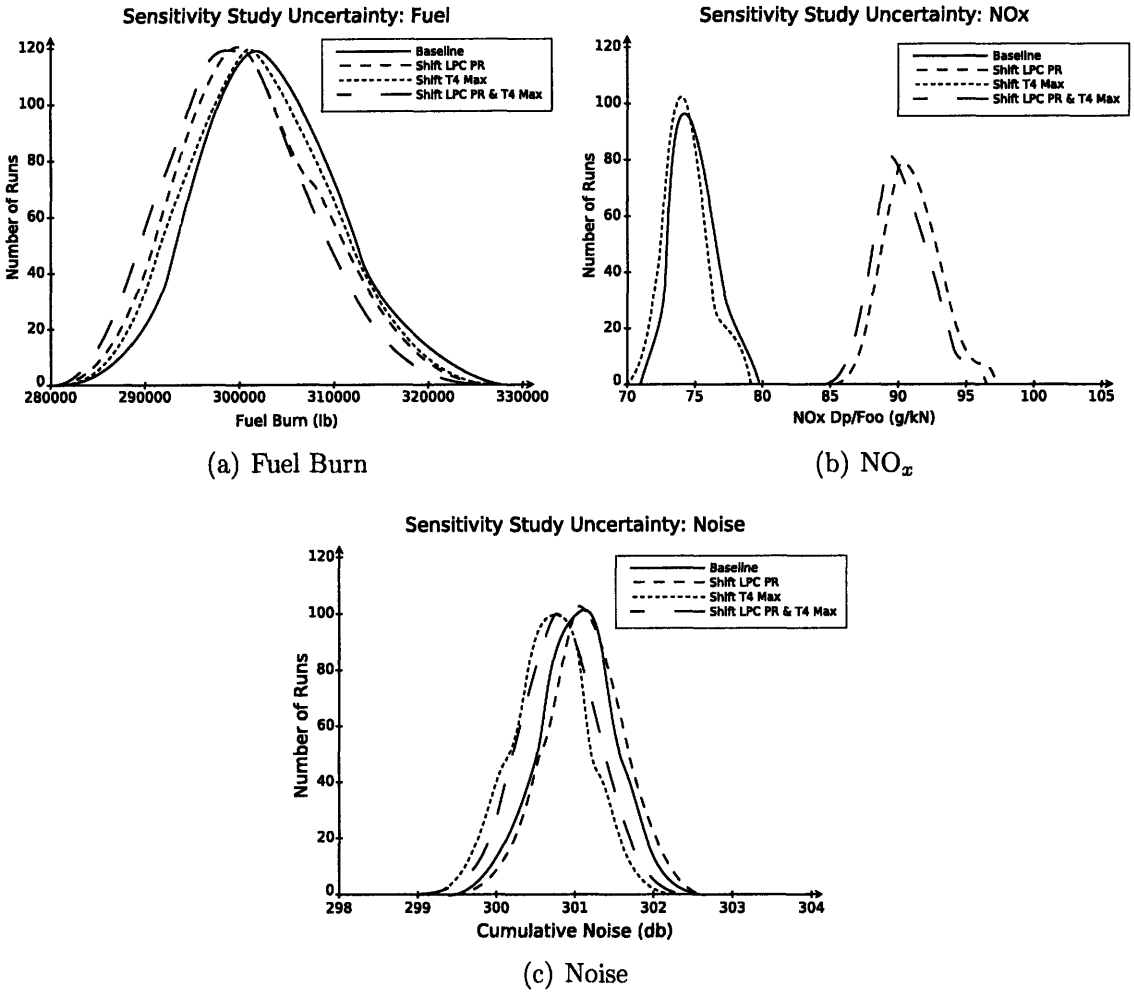

(a) Fuel Burn

(b) NO_x

(c) Noise

Figure 4-14: Sensitivity Study Uncertainty Output Distributions

Figure 4-14 shows the uncertainty distributions of fuel burn, LTO-NO_x emissions, and noise for the four cases in this study. The plot of LTO-NO_x shows that changing LPC pressure ratio causes a mean shift in the NO_x emission distribution. While the uncertainty in the shifted LPC curve is about the same as the baseline curve, the uncertainty in the shift is decreased by 77% when compared to the baseline uncertainty.

Similar to the LTO-NO_x plot, the graph of noise shows a mean shift when T4 is changed. The standard deviation in noise for the baseline case is 0.167% of the

baseline mean and the standard deviation in noise for the shifted T4 case is 0.176% of the shifted T4 case mean. The shift in T4 causes a 0.104% mean decrease in noise. This is an ideal example of a small mean shift that would normally be obscured in uncertainty. Since all the inputs except for T4 have the same distributions in both cases, the distributions can be subtracted. The uncertainty of the shift is decreased by 42% when compared to the baseline uncertainty.

The standard deviation of fuel for the both the baseline and shifted LPC cases is 2.4% of the mean value. When LPC is changed there is a 0.61% decrease in fuel burn. This shift would normally not be distinguishable from the uncertainty but since the same input uncertainties were used for most the inputs, the uncertainty of the change in LPC only 0.09%. This shows that EDS is capable of answering questions of higher confidence than one would assume from looking at a single uncertainty study specifically when looking at sensitivity and trade studies.

Chapter 5

Conclusion and Future Work

5.1 Conclusion

The model assessment study showed that the major discrepancy between EDS and the PW design methodology is that PW uses a three point engine design. This result was also found during a similar study with GEAE which indicates that using a three point design is a typical industry practice. As shown in Section 3.4.1, switching to a three point design method improves EDS's ability to match the trends predicted by industry engine models.

The input sensitivity study showed that there are a few key drivers to the EDS model, most of which are variables one would expect such as design range, cruise Mach number, wing area, aspect ratio, and engine pressure ratios. However, the direction of the trends with some of these variables is counterintuitive due to the typical industry practice constraint that the aircraft thrust to weight ratio is held constant as discussed in Section 4.3.

The constraint sensitivity study revealed that there are only a handful of constraints implemented in EDS and that the current method for applying additional constraints after running a design of experiments can increase the resultant errors due to the response surfaces used. As shown with a simplified example, fitting response surfaces to results before constraints are applied can cause substantial error. In general, constraints can affect design decisions a great deal and care is needed in

handling them when creating response surfaces

The uncertainty studies revealed the implications of attempting to fix cases which would otherwise fail with an example of the fan map Rline fix. Although the fix does allow more cases to run successfully it is done by changing the fan performance which can skew any results obtained. In addition the fan map Rline fix increases the output uncertainty. For these reasons, the fan map Rline fix should be removed from EDS.

Finally, the trade study uncertainty analysis showed that EDS is capable of answering questions with higher confidence than one would assume from the results of the input uncertainty study since the uncertainty due to variables which are not changing in a trade study are not significant.

5.2 Future Work

The most important continuing effort from this work is to complete the implementation of a three point design method in EDS. Since this methodology is a typical industry practice, it is imperative that EDS use it to be able to produce accurate trade studies. Also along the lines of EDS development are the issues surrounding the fan map fix. The fan map fix should be removed from EDS since it implies that the components include variable geometry which is beyond the technology limits of interest for EDS. In addition, a flag should be set to indicate when any of the fixes are implemented so those cases can be filtered out later if they are causing unexpected trends in the results.

Another key result was the realization that applying constraints after the response surfaces are fit to design of experiments results can lead to greater errors. Although the differences were small when only one constraint was investigated, the error should be reduced more significantly on a design of experiments with more than two degrees of freedom. This phenomenon should be further investigated to see if the additional errors are acceptable or if other response surface methodologies alleviate this problem. In addition, a standard list of constraints for use with EDS trade studies should be compiled even if they are not implemented until after EDS is run.

Further assessment of the EDS model input uncertainty should be performed. Since each EDS model is supposed to represent an aircraft size class as opposed to a single specific aircraft, the input distribution ranges should be independently based on how each parameter varies within an aircraft class. The uncertainties also need to be better understood by performing global sensitivity studies for each of the inputs.

A final aspect of EDS which requires further attention is the inconsistent case failures. Consider an example study in which BPR is varied from 7 to 10 in 0.1 increments. The cases up to 8.7 and past 8.9 may run fine but when BPR is 8.8 EDS will fail for no physical reason in the aircraft model. This type of response was apparent in many of the sensitivity studies. Failures will often happen at a few seemingly random locations in the design space but they are reproducible. Since these failures are due to the model implementation and not the physics of the model, they should be flagged as a known problem and resolved in future versions of EDS.

Appendix A

EDS Input Variables

Table A.1 lists the EDS inputs varied for this thises. The table includes the input name, a description of the input, the input value for the baseline model, the minimum and maximum values used to define the uncertainty range, the uncertainty distribution shape factors α and β, and if the input was held constant during the Monte Carlo simulations.

Table A.1: EDS Input Variables

	Input Name	Input Description	Units	Baseline Value	Minimum	Maximum	α	β	Held Constant
1	Ambient_alt	Ambient Altitude	ft	0.00	0.00	15.00	0.5	2	
2	Ambient_MN	Ambient Mach Number		0.00	0.00	0.02	0.5	2	
3	Ambient_dTamb	Ambient Delta Temperature	F	27.00	26.60	27.41	10	10	
4	Ambient_W	Inlet Air Mass Flow	lb/s	2616.67	2577.42	2655.92	10	10	
5	WATE_AccWtEngWtRatio	Engine Accessory Weight	lb	740.00	728.90	751.10	10	10	
6	Inlet_Afs	Inlet Area	in2	3500.00	3447.50	3552.50	10	10	Yes
7	Inlet_Fl_O_MN	Inlet Flow Mach Number		0.630	0.621	0.639	10	10	Yes
8	Inlet_Wate_MNin	Inlet Mach Number		0.850	0.837	0.863	10	10	
9	Inlet_Wate_shapeFactor	Inlet Shape Factor		1.000	0.985	1.015	10	10	Yes
10	Inlet_Wate_engMountFactor	Inlet Engine Mount Factor		1.000	0.985	1.015	10	10	
11	Inlet_Wate_LDratio	Inlet Length to Diameter Ratio		0.382	0.376	0.387	10	10	
12	k_Inl_Wt	Inlet Weight Adjustment Factor		0.000	-0.004	0.004	10	10	
13	Inlet_Wate_nacelleDensity	Nacelle Material Density	lb/in3	0.060	0.060	0.060	10	10	
14	Inlet_Wate_linerDensity	Inlet Liner Material Density	lb/in3	0.090	0.090	0.090	10	10	
15	Inlet_Wate_linerThickness	Inlet Liner Thickness	in	0.104	0.104	0.104	10	10	
16	Inlet_Wate_nacelleWallThickness	Inlet Nacelle Wall Thickness	in	14.07	14.02	14.12	10	10	
17	Inlet_Wate_engUltLoadFactor	Engine Ultimate Load Factor		2.000	1.993	2.008	10	10	
18	k_Fan_PolyEff	Fan Efficiency Adjustment Factor		-0.010	-0.030	0.004	10	2	
19	Fan_Fl_O_MN	Fan Mach Number		0.450	0.443	0.457	10	10	
20	Fan_S_map_alpha	Fan Map Angle		0.000	0.000	0.000	10	10	
21	Fan_S_map_RlineMap	Fan Map Design Rline		2.200	2.167	2.233	10	10	
22	Fan_S_map_NcDes	Fan Map Design Corrected Speed		0.975	0.960	0.990	10	10	
23	Fan_S_map_PRdes	Fan Map Design Pressure Ratio		1.700	1.675	1.726	10	10	
24	Fan_S_map_effDes	Fan Map Design Efficiency		0.890	-0.030	0.004	10	2	
25	Fan_Wate_MNin	Fan Inlet Mach Number		0.655	0.645	0.665	10	10	
26	Fan_Wate_MNout	Fan Outlet Mach Number		0.500	0.493	0.508	10	10	
27	Fan_Wate_FSmaxPR	Fan First Stage Max Pressure Ratio		1.800	1.773	1.827	10	10	Yes
28	Fan_Wate_outletInletRR	Fan Outlet to Inlet Radius Ratio		1.000	0.985	1.015	10	10	Yes
29	Fan_Wate_inletRR	Fan Inlet Hub to Tip Ratio		0.314	0.309	0.319	10	10	
30	k_Fan_Wt	Fan Weight Adjustment Factor		0.000	-0.004	0.004	10	10	
31	Fan_Wate_numRotorBlades	Fan Number of Rotor Blades		22.00	21.00	23.00	2	2	
32	Fan_Wate_bladeDensity	Fan Blade Material Density	lb/in3	0.096	0.096	0.096	10	10	
33	Fan_Wate_bladeSolidity	Fan Blade Solidity		1.500	1.478	1.523	10	10	Yes
34	Fan_Wate_bladeVolumeFactor	Fan Blade Volume Factor		0.024	0.024	0.024	10	10	
35	Fan_Wate_FSbladeAR	Fan First Stage Blade Aspect Ratio		2.070	2.039	2.101	10	10	
36	Fan_Wate_LSbladeAR	Fan Last Stage Blade Aspect Ratio		2.070	2.039	2.101	10	10	Yes

Continued on Next Page...

Table A.1 – Continued

	Input Name	Input Description	Units	Baseline Value	Minimum	Maximum	α	β	Held Constant
37	Fan_Wate_bladeTaperRatio	Fan Blade Taper Ratio		1.400	1.379	1.421	10	10	Yes
38	Fan_Wate_numStatorBlades	Fan Number of Stator Blades		50.00	49.00	51.00	2	2	
39	Fan_Wate_statorDensity	Fan Stator Material Density	lb/in3	0.100	0.100	0.100	10	10	
40	Fan_Wate_statorVolumeFactor	Fan Stator Volume Factor		0.140	0.139	0.141	10	10	
41	Fan_Wate_FSstatorAR	Fan First Stage Stator Aspect Ratio		3.800	3.743	3.857	10	10	
42	Fan_Wate_LSstatorAR	Fan Last Stage Stator Aspect Ratio		3.800	3.743	3.857	10	10	Yes
43	Fan_Wate_rotorStatorDuct	Fan Duct Length to Rotor Axial Length		0.350	0.345	0.355	10	10	
44	Fan_Wate_rotorStatorDuctBypass	Fan Bypass Duct to Rotor Axial Length Ratio		-0.200	-0.197	-0.203	10	10	
45	Fan_Wate_containmentDensity	Fan Containment Material Density	lb/in3	0.035	0.035	0.035	10	10	
46	Fan_Wate_caseDensity	Fan Case Material Density	lb/in3	0.100	0.100	0.100	10	10	
47	Fan_Wate_s_gearboxWt	Fan Gear Box Weight	lb	1.000	0.996	1.004	10	10	Yes
48	Fan_Wate_s_Nmech	Fan Mechanical Speed		1.000	0.985	1.015	10	10	Yes
49	k_Fan_TS	Fan Tip Speed Adjustment Factor		1.144	1.126	1.161	10	10	
50	Fan_Wate_avgLengthPerStage	Fan Average Length Per Stage		18.80	18.52	19.08	10	10	
51	Fan_S_RearFrame_density	Fan Rear Frame Material Density	lb/in3	0.100	0.100	0.100	10	10	
52	Fan_S_RearFrame_volumeFactor	Fan Rear Frame Volume Factor		0.050	0.050	0.050	10	10	
53	Fan_S_RearFrame_aspectRatio	Fan Rear Frame Aspect Ratio		2.250	2.216	2.284	10	10	
54	Fan_S_RearFrame_numBlades	Fan Rear Frame Number of Blades		5.000	4.000	6.000	2	2	
55	Fan_S_RearFrame_supportDensity	Fan Rear Frame Support Density Factor		0.100	0.100	0.100	10	10	
56	Fan_S_RearFrame_supportThickness	Fan Rear Frame Support Thickness Factor		0.100	0.100	0.100	10	10	
57	Fan_S_RearFrame_gapFrameLengthRatio	Fan Rear Frame Gap Length Ratio		0.200	0.197	0.203	10	10	Yes
58	Fan_S_RearFrame_HPX	Fan Rear Frame Horsepower Extraction		500.00	492.50	507.50	10	10	Yes
59	Fan_S_RearFrame_towerShaftDiaRatio	Fan Rear Frame Shaft Diameter Ratio		0.900	0.887	0.914	10	10	Yes
60	Splitter_Fl_PO_MN	Splitter Primary (Core) Flow Mach Number		0.450	0.443	0.457	10	10	Yes
61	Splitter_Fl_SO_MN	Splitter Secondary (Bypass) Flow Mach Number		0.450	0.443	0.457	10	10	Yes
62	k_Splitter_Wt	Splitter Weight Adjustment Factor		0.000	0.000	0.000	10	10	Yes
63	Duct4_Fl_O_MN	Fan/LPC Duct Flow Mach Number		0.400	0.394	0.406	10	10	Yes
64	Duct4_Wate_MNin	Fan/LPC Inlet Mach Number		0.460	0.453	0.467	10	10	Yes
65	Duct4_Wate_lengthHeightRatio	Fan/LPC Duct Length to Height Ratio		0.500	0.493	0.508	10	10	Yes
66	k_Duct4_Wt	Fan/LPC Duct Weight Adjustment Factor		0.000	0.000	0.000	10	10	Yes
67	Duct4_Wate_length	Fan/LPC Duct Length to Height Ratio		0.100	0.099	0.102	10	10	Yes
68	k_LPC_PolyEff	LPC Efficiency Adjustment Factor		-0.008	-0.030	0.004	10	2	
69	LPC_Fl_O_MN	LPC Flow Mach Number		0.400	0.394	0.406	10	10	Yes
70	LPC_S_map_RlineMap	LPC Map Design Rline		2.400	2.364	2.436	10	10	
71	LPC_S_map_NcDes	LPC Map Design Corrected Speed		0.980	0.965	0.995	10	10	
72	LPC_S_map_PRdes	LPC Map Design Pressure Ratio		2.423	2.386	2.459	10	10	
73	LPC_S_map_effDes	LPC Map Design Efficiency		0.900	-0.030	0.004	10	2	

Continued on Next Page...

Table A.1 – Continued

	Input Name	Input Description	Units	Baseline Value	Minimum	Maximum	α	β	Held Constant
74	LPC_Wate_MNin	LPC Inlet Mach Number		0.470	0.463	0.477	10	10	
75	LPC_Wate_MNout	LPC Outlet Mach Number		0.430	0.424	0.436	10	10	
76	LPC_Wate_FSmaxPR	LPC First Stage Max Pressure Ratio		1.200	1.182	1.218	10	10	Yes
77	LPC_Wate_outletInletRR	LPC Outlet to Inlet Radius Ratio		0.900	0.887	0.914	10	10	
78	LPC_Wate_inletRR	LPC Inlet Hub to Tip Ratio		0.700	0.690	0.711	10	10	
79	k_LPC_Wt	LPC Weight Adjustment Factor		0.000	-0.004	0.004	10	10	
80	LPC_Wate_bladeSolidity	LPC Blade Solidity		0.895	0.882	0.908	10	10	
81	LPC_Wate_FSbladeAR	LPC First Stage Blade Aspect Ratio		2.650	2.610	2.690	10	10	
82	LPC_Wate_LSbladeAR	LPC Last Stage Blade Aspect Ratio		1.700	1.675	1.726	10	10	
83	LPC_Wate_statorSolidity	LPC Stator Solidity		1.240	1.221	1.259	10	10	
84	LPC_Wate_FSstatorRotorLR	LPC First Stage Stator to Rotor Length Ratio		0.600	0.591	0.609	10	10	
85	LPC_Wate_LSstatorRotorLR	LPC Last Stage Stator to Rotor Length Ratio		1.000	0.985	1.015	10	10	
86	LPC_Wate_IGVsolidity	LPC Inlet Guide Vane Solidity		1.540	1.517	1.563	10	10	
87	LPC_Wate_IGV_AR	LPC Inlet Guide Vane Aspect Ratio		1.500	1.478	1.523	10	10	
88	LPC_Wate_s_gearboxWt	LPC Gear Box Weight Adjustment Factor		1.000	0.996	1.004	10	10	Yes
89	LPC_Wate_s_Nmech	LPC Mechanical Speed Factor		1.000	0.985	1.015	10	10	Yes
90	LPC_Wate_avgLengthPerStage	LPC Average Length per Stage	in	5.250	5.171	5.329	10	10	
91	Duct6_Fl_O_MN	LPC/HPC Duct Flow Mach Number		0.450	0.443	0.457	10	10	Yes
92	Duct6_Wate_MNin	LPC/HPC Duct Inlet Mach Number		0.300	0.296	0.305	10	10	Yes
93	Duct6_Wate_lengthHeightRatio	LPC/HPC Duct Length to Height Ratio		2.350	2.315	2.385	10	10	Yes
94	k_Duct6_Wt	LPC/HPC Duct Weight Adjustment Factor		0.000	-0.015	0.015	10	10	
95	Duct6_Wate_frameAspectRatio	LPC/HPC Duct Frame Aspect Ratio		1.000	0.985	1.015	10	10	Yes
96	Duct6_Wate_length	LPC/HPC Duct Length	in	13.00	12.81	13.20	10	10	
97	Duct6_S_Frame_density	LPC/HPC Duct Frame Material Density	lb/in3	0.160	0.159	0.161	10	10	
98	Duct6_S_Frame_volumeFactor	LPC/HPC Duct Frame Volume Factor		0.050	0.050	0.050	10	10	
99	Duct6_S_Frame_numBlades	LPC/HPC Duct Frame Number of Blades		48.00	47.00	49.00	2	2	
100	Duct6_S_Frame_supportDensity	LPC/HPC Duct Frame Support Material Density	lb/in3	0.160	0.159	0.161	10	10	
101	Duct6_S_Frame_supportThickness	LPC/HPC Duct Frame Support Thickness	in	0.100	0.100	0.100	10	10	
102	Duct6_S_Frame_gapFrameLengthRatio	LPC/HPC Duct Frame Gap Length Ratio		0.200	0.197	0.203	10	10	Yes
103	k_HPC_PolyEff	HPC Efficiency Factor		-0.008	-0.030	0.004	10	2	
104	HPC_Fl_O_MN	HPC Flow Mach Number		0.300	0.296	0.305	10	10	Yes
105	HPC_BleedFlow	HPC Bleed Flow		3.930	3.871	3.989	10	10	Yes
106	HPC_S_map_RlineMap	HPC Map Design Rline		1.900	1.872	1.929	10	10	
107	HPC_S_map_NcDes	HPC Map Design Corrected Speed		1.000	0.985	1.015	10	10	
108	HPC_S_map_PRdes	HPC Map Design Pressure Ratio		9.800	9.653	9.947	10	10	
109	HPC_S_map_effDes	HPC Map Design Efficiency		0.879	-0.030	0.004	10	2	
110	HPC_Cool1_fracBldWork	HPC Cooling Flow 1 Work Fraction		0.350	0.345	0.355	10	10	

Continued on Next Page...

Table A.1 – Continued

	Input Name	Input Description	Units	Baseline Value	Minimum	Maximum	α	β	Held Constant
111	HPC_Cool1_fracBldP	HPC Cooling Flow 1 Pressure Fraction		0.147	0.144	0.149	10	10	Yes
112	HPC_Cool1_fracBldW	HPC Cooling Flow 1 Weight Fraction		0.011	0.011	0.011	10	10	
113	HPC_Cool2_fracBldWork	HPC Cooling Flow 2 Work Fraction		0.350	0.345	0.355	10	10	
114	HPC_Cool2_fracBldP	HPC Cooling Flow 2 Pressure Fraction		0.147	0.144	0.149	10	10	Yes
115	HPC_Cool2_fracBldW	HPC Cooling Flow 2 Weight Fraction		0.006	0.006	0.006	10	10	Yes
116	HPC_CustBld_fracBldWork	HPC Customer Bleed Work Fraction		0.350	0.345	0.355	10	10	
117	HPC_CustBld_fracBldP	HPC Customer Bleed Pressure Fraction		0.147	0.144	0.149	10	10	Yes
118	HPC_Wate_MNin	HPC Inlet Mach Number		0.410	0.404	0.416	10	10	
119	HPC_Wate_MNout	HPC Outlet Mach Number		0.270	0.266	0.274	10	10	
120	HPC_Wate_FSmaxPR	HPC First Stage Max Pressure Ratio		1.350	1.330	1.370	10	10	
121	HPC_Wate_outletInletRR	HPC Outlet to Inlet Radius Ratio		0.800	0.788	0.812	10	10	
122	HPC_Wate_inletRR	HPC Inlet Hub to Tip Ratio		0.664	0.654	0.674	10	10	
123	k_HPC_Wt	HPC Weight Adjustment Factor		0.000	-0.004	0.004	10	10	
124	HPC_Wate_bladeSolidity	HPC Blade Solidity		1.100	1.084	1.117	10	10	
125	HPC_Wate_bladeVolumeFactor	HPC Blade Volume Factor		0.143	0.142	0.144	10	10	
126	HPC_Wate_FSbladeAR	HPC First Stage Blade Aspect Ratio		1.700	1.675	1.726	10	10	
127	HPC_Wate_LSbladeAR	HPC Last Stage Blade Aspect Ratio		1.340	1.320	1.360	10	10	
128	HPC_Wate_statorSolidity	HPC Stator Solidity		1.270	1.251	1.289	10	10	
129	HPC_Wate_statorVolumeFactor	HPC Stator Volume Factor		0.440	0.438	0.442	10	10	
130	HPC_Wate_FSstatorRotorLR	HPC First Stage Stator to Rotor Length Ratio		0.495	0.488	0.502	10	10	
131	HPC_Wate_LSstatorRotorLR	HPC Last Stage Stator to Rotor Length Ratio		1.820	1.793	1.847	10	10	
132	HPC_Wate_numVariableStages	HPC Number of Variable Stages		3.000	2.000	4.000	2	2	
133	HPC_Wate_caseDensity	HPC Case Material Density	lb/in3	0.290	0.289	0.291	10	10	
134	HPC_Wate_s_gearboxWt	HPC Gear Box Weight Factor		1.000	0.996	1.004	10	10	Yes
135	HPC_Wate_s_Nmech	HPC Mechanical Speed		1.000	0.985	1.015	10	10	Yes
136	k_HPC_TS	HPC Tip Speed Adjustment Factor		1.057	1.041	1.073	10	10	
137	HPC_Wate_diskBoreBladeHubRR	HPC Disk Bore to Airfoil Hub Radius Ratio		0.390	0.384	0.396	10	10	
138	HPC_Wate_avgLengthPerStage	HPC Average Length per Stage	in	3.120	3.073	3.167	10	10	
139	HPC_Wate_minHubRadius	HPC Min Hub Radius	in	9.300	9.161	9.440	10	10	Yes
140	Bld3_Fl_O_MN	Bleed Flow Mach Number		0.300	0.296	0.305	10	10	Yes
141	Bld3_Cool1_fracW	Cooling Flow 1 Bleed to Element Inlet Flow Ratio		0.120	0.118	0.122	10	10	
142	Bld3_Cool2_fracW	Cooling Flow 2 Bleed to Element Inlet Flow Ratio		0.070	0.069	0.071	10	10	Yes
143	Bld3_Wate_MNin	Bleed Inlet Mach Number		0.270	0.266	0.274	10	10	Yes
144	Bld3_Wate_lengthHeightRatio	Bleed Length to Height Ratio		6.000	5.910	6.090	10	10	Yes
145	k_Bld3_Wt	Bleed Weight Adjustment Factor		0.000	-0.004	0.004	10	10	
146	Bld3_Wate_length	Bleed Length	in	9.200	9.062	9.338	10	10	
147	FUEL36_LHV	Fuel Heating Value	BTU/lb	18400	18124	18676	10	10	

Continued on Next Page...

Table A.1 – Continued

	Input Name	Input Description	Units	Baseline Value	Minimum	Maximum	α	β	Held Constant
148	Burner_effBase	Burner Efficiency		0.999	0.997	1.001	2	0.5	
149	Burner_Fl_O_MN	Burner Flow Mach Number		0.100	0.099	0.102	10	10	Yes
150	Burner_FAR	Burner Fuel to Air Ratio		0.029	0.028	0.029	10	10	
151	Burner_TtCombOut	Burner Exit Temperature	R	3500.0	3447.5	3552.5	10	10	Yes
152	Burner_Emissions_delphi	Burner Emissions Factor		0.750	0.739	0.761	10	10	Yes
153	Burner_Emissions_PCT_Reduction	Burner Emissions Factor		0.307	0.302	0.312	10	10	Yes
154	Burner_Wate_Vflow	Burner Flow Velocity	ft/s	75.00	73.88	76.13	10	10	
155	Burner_Wate_residenceTime	Burner Residence Time	s	0.011	0.011	0.011	10	10	
156	k_burner_Wt	Burner Weight Adjustment Factor		0.000	-0.004	0.004	10	10	
157	k_Burner_linerDensity	Burner Liner Material Density	lb/in3	0.000	-0.004	0.004	10	10	
158	Burner_Wate_caseDensity	Burner Case Material Density	lb/in3	0.322	0.321	0.323	10	10	
159	Max_T4_eq_rhs	Maximum Turbine Inlet Temperature	R				10	10	
160	HPT_Fl_O_MN	HPT Flow Mach Number		0.300	0.296	0.305	10	10	Yes
161	k_HPT_AddEff	HPT Efficiency Adjustment Factor		-0.003	-0.030	0.004	10	2	
162	HPT_S_map_parmMap	HPT Map Parameter		5.280	5.201	5.359	10	10	
163	HPT_S_map_parmMapDes	HPT Map Design Map Parameter		4.800	4.728	4.872	10	10	
164	HPT_S_map_parmNcDes	HPT Map Design Speed		100.00	98.50	101.50	10	10	
165	k_HPT_desVaneTemp1	HPT Vane 1 Design Temperature Delta	R	0.0	-15.0	15.0	10	10	
166	k_HPT_desVaneTemp2	HPT Vane 2 Design Temperature Delta	R	0.0	-15.0	15.0	10	10	
167	k_HPT_desBladeTemp	HPT Blade Design Temperature Delta	R	0.0	-15.0	15.0	10	10	
168	HPT_Cool_xFactor	HPT Cooling Factor 1		0.484	0.477	0.492	10	10	
169	HPT_Cool_xFactor1	HPT Cooling Factor 2		1.467	1.445	1.489	10	10	
170	custbleed	Customer Bleed Factor		0.012	0.012	0.012	10	10	
171	HPT_Wate_MNin	HPT Inlet Mach Number		0.092	0.091	0.093	10	10	
172	HPT_Wate_MNout	HPT Outlet Mach Number		0.270	0.266	0.274	10	10	
173	HPT_Wate_loadingParameter	HPT Loading Parameter		0.342	0.336	0.347	10	10	Yes
174	k_HPT_GEload	HPT GE Loading Parameter Factor		0.200	0.197	0.203	10	10	
175	HPT_Wate_numberOfStages	HPT Number of Stages		2.000	1.000	3.000	2	2	
176	k_HPT_Wt	HPT Weight Adjustment Factor		0.000	-0.004	0.004	10	10	
177	HPT_Wate_bladeDensity	HPT Blade Material Density	lb/in3	0.312	0.311	0.313	10	10	
178	HPT_Wate_bladeSolidity	HPT Blade Solidity		0.829	0.817	0.841	10	10	
179	HPT_Wate_bladeVolumeFactor	HPT Blade Volume Factor		0.590	0.588	0.592	10	10	
180	HPT_Wate_FSbladeAR	HPT First Stage Blade Aspect Ratio		1.900	1.872	1.929	10	10	
181	HPT_Wate_LSbladeAR	HPT Last Stage Blade Aspect Ratio		2.400	2.364	2.436	10	10	
182	HPT_Wate_statorDensity	HPT Stator Material Density	lb/in3	0.312	0.311	0.313	10	10	
183	HPT_Wate_statorSolidity	HPT Stator Solidity		0.762	0.751	0.773	10	10	
184	HPT_Wate_statorVolumeFactor	HPT Stator Volume Factor		0.590	0.588	0.592	10	10	

Continued on Next Page...

Table A.1 – Continued

	Input Name	Input Description	Units	Baseline Value	Minimum	Maximum	α	β	Held Constant
185	HPT_Wate_FSstatorRotorLR	HPT First Stage Stator to Rotor Length Ratio		1.450	1.428	1.472	10	10	
186	HPT_Wate_LSstatorRotorLR	HPT Last Stage Stator to Rotor Length Ratio		1.600	1.576	1.624	10	10	
187	HPT_Wate_caseDensity	HPT Case Material Density	lb/in3	0.287	0.286	0.288	10	10	
188	HPT_Wate_diskDensity	HPT Disk Material Density	lb/in3	218.00	217.18	218.82	10	10	
189	HPT_Wate_diskRefStress	HPT Disk Reference Stress	lbf/in2	100000	98500	101500	10	10	Yes
190	HPT_Wate_TmaxMetal	HPT Max Disk Metal Temperature	R	1660.0	1635.1	1684.9	10	10	
191	HPT_Wate_avgLengthPerStage	HPT Average Length per Stage	in	4.300	4.236	4.365	10	10	
192	ATD_Bleed_Fl_O_MN	ATD Bleed Flow Mach Number		0.300	0.296	0.305	10	10	Yes
193	ATD_Bleed_Wate_MNin	ATD Bleed Inlet Mach Number		0.270	0.266	0.274	10	10	Yes
194	Duct11_Fl_O_MN	HPT/LPT Duct Flow Mach Number		0.300	0.296	0.305	10	10	Yes
195	Duct11_Wate_MNin	HPT/LPT Duct Inlet Mach Number		0.270	0.266	0.274	10	10	Yes
196	Duct11_Wate_lengthHeightRatio	HPT/LPT Duct Length to Height Ratio		1.750	1.724	1.776	10	10	Yes
197	k_Duct11_Wt	HPT/LPT Duct Weight Adjustment Factor		0.000	-0.004	0.004	10	10	
198	Duct11_Wate_length	HPT/LPT Duct Length	in	4.600	4.531	4.669	10	10	
199	Poly_LPT_Eff_eq_rhs	LPT Design Efficiency		0.915	0.901	0.929	10	10	Yes
200	LPT_Fl_O_MN	LPT Flow Mach Number		0.350	0.345	0.355	10	10	Yes
201	k_LPT_AddEff	LPT Efficiency Adjustment Factor		-0.003	-0.030	0.004	10	2	
202	LPT_S_map_parmMap	LPT Map Parameter		5.010	4.935	5.085	10	10	
203	LPT_S_map_parmMapDes	LPT Map Design Map Parameter		5.500	5.418	5.583	10	10	
204	LPT_S_map_parmNcDes	LPT Map Design Corrected Speed		100.00	98.50	101.50	10	10	
205	k_LPT_desVaneTemp	LPT Vane Temperature Delta	R	0.000	0.000	0.000	10	10	Yes
206	k_LPT_desBladeTemp	LPT Blade Temperature Delta	R	0.000	0.000	0.000	10	10	Yes
207	LPT_Cool_xFactor	LPT Cooling Factor 1		0.640	0.630	0.650	10	10	
208	LPT_Cool_xFactor1	LPT Cooling Factor 2		1.208	1.190	1.226	10	10	
209	LPT_Wate_MNin	LPT Inlet Mach Number		0.280	0.276	0.284	10	10	
210	LPT_Wate_MNout	LPT Outlet Mach Number		0.340	0.335	0.345	10	10	
211	LPT_Wate_loadingParameter	LPT Loading Parameter		0.230	0.227	0.233	10	10	Yes
212	k_LPT_GEload	LPT GE Loading Parameter Adjustment Factor		0.150	0.148	0.152	10	10	
213	LPT_Wate_outletInletRR	LPT Outlet to Inlet Radius Ratio		1.300	1.281	1.320	10	10	
214	k_LPT_Wt	LPT Weight Adjustment Factor		0.000	-0.004	0.004	10	10	
215	LPT_Wate_bladeDensity	LPT Blade Material Density	lb/in3	0.313	0.312	0.314	10	10	
216	LPT_Wate_bladeSolidity	LPT Blade Solidity		1.450	1.428	1.472	10	10	
217	LPT_Wate_bladeVolumeFactor	LPT Blade Volume Factor		0.190	0.189	0.191	10	10	
218	LPT_Wate_FSbladeAR	LPT First Stage Blade Aspect Ratio		2.850	2.807	2.893	10	10	
219	LPT_Wate_LSbladeAR	LPT Last Stage Blade Aspect Ratio		3.320	3.270	3.370	10	10	
220	LPT_Wate_statorDensity	LPT Stator Material Density, lbm/in3	lb/in3	0.313	0.312	0.314	10	10	
221	LPT_Wate_statorVolumeFactor	LPT Stator Volume Factor		0.150	0.149	0.151	10	10	

Continued on Next Page...

Table A.1 – Continued

	Input Name	Input Description	Units	Baseline Value	Minimum	Maximum	α	β	Held Constant
222	LPT_Wate_FSstatorRotorLR	LPT First Stage Stator to Rotor Length Ratio		1.550	1.527	1.573	10	10	
223	LPT_Wate_LSstatorRotorLR	LPT Last Stage Stator to Rotor Length Ratio		0.693	0.683	0.703	10	10	
224	LPT_Wate_caseDensity	LPT Case Material Density	lb/in3	0.300	0.299	0.301	10	10	
225	LPT_Wate_diskDensity	LPT Disk Material Density	lb/in3	218.00	217.18	218.82	10	10	
226	LPT_Wate_diskRefStress	LPT Disk Reference Stress	lbf/in2	100000	98500	101500	10	10	Yes
227	LPT_Wate_TmaxMetal	LPT Max Disk Metal Temperature	R	1660.0	1635.1	1684.9	10	10	
228	LPT_Wate_diskBoreBladeHubRR	LPT Disk bore radius to the airfoil hub radius ratio		0.690	0.680	0.700	10	10	
229	LPT_Wate_bladeDensity2	LPT Blade Material 2 Density	lb/in3	0.286	0.282	0.290	10	10	
230	LPT_Wate_statorDensity2	LPT Stator Material 2 Density	lb/in3	0.286	0.282	0.290	10	10	
231	LPT_Wate_avgLengthPerStage	LPT Average Length per Stage	in	5.790	5.703	5.877	10	10	
232	LPT_S_Frame_density	LPT Frame Material Density	lb/in3	0.297	0.296	0.298	10	10	
233	LPT_S_Frame_volumeFactor	LPT Frame Volume Factor		0.050	0.050	0.050	10	10	
234	LPT_S_Frame_aspectRatio	LPT Frame Aspect Ratio		1.450	1.428	1.472	10	10	
235	LPT_S_Frame_numBlades	LPT Frame Number of Blades		28.00	27.00	29.00	2	2	
236	LPT_S_Frame_supportDensity	LPT Frame Support Material Density	lb/in3	0.297	0.296	0.298	10	10	
237	LPT_S_Frame_supportThickness	LPT Frame Support Thickness	in	0.100	0.100	0.100	10	10	
238	LPT_S_Frame_gapFrameLengthRatio	LPT Frame Gap Length Ratio		0.200	0.197	0.203	10	10	
239	Duct13_Fl_O_MN	LPT/Nozzle Duct Flow Mach Number		0.250	0.246	0.254	10	10	Yes
240	Duct13_Wate_MNin	LPT/Nozzle Duct Inlet Mach Number		0.250	0.246	0.254	10	10	Yes
241	Duct13_Wate_lengthHeightRatio	LPT/Nozzle Duct Length to Height Ratio		0.520	0.512	0.528	10	10	Yes
242	k_Duct13_Wt	LPT/Nozzle Duct Weight Adjustment Factor		0.000	-0.004	0.004	10	10	
243	Duct13_Wate_length	LPT/Nozzle Duct Length	in	2.000	1.970	2.030	10	10	
244	BypBld_Lkg_fracW	Bypass Bleed Leakage Weight Fraction		0.005	0.005	0.005	10	10	
245	BypBld_Fl_O_MN	Bypass Bleed Flow Mach Number		0.450	0.443	0.457	10	10	Yes
246	k_BypBld_Wt	Bypass Bleed Weight Adjustment Factor		0.000	0.000	0.000	10	10	Yes
247	Duct15_Fl_O_MN	Bypass/Nozzle Duct Flow Mach Number		0.450	0.443	0.457	10	10	Yes
248	Duct15_Wate_MNin	Bypass/Nozzle Duct Inlet Mach Number		0.480	0.473	0.487	10	10	Yes
249	Duct15_Wate_lengthHeightRatio	Bypass/Nozzle Duct Length to Height Ratio		1.200	1.182	1.218	10	10	Yes
250	k_Duct15_Wt	Bypass/Nozzle Duct Weight Adjustment Factor		0.000	-0.004	0.004	10	10	
251	Duct15_Wate_density	Bypass/Nozzle Duct Material Density	lb/in3	0.100	0.100	0.100	10	10	
252	Core_Nozz_Cv	Core Nozzle Exit Velocity Loss Coefficient		1.000	0.992	1.000	2	1	
253	Core_Nozz_Wate_LDratio	Core Nozzle Length to Diameter Ratio		0.270	0.266	0.274	10	10	
254	Core_Nozz_Wate_exitArea	Core Nozzle Exit Area	in2	3700.0	3644.5	3755.5	10	10	Yes
255	Core_Nozz_Wate_nozzlePlugLR	Core Nozzle to Plug Length Ratio		4.000	3.940	4.060	10	10	
256	k_Core_Wt	Core Nozzle Weight Adjustment Factor		0.000	-0.004	0.004	10	10	
257	Core_Nozz_Wate_plugDensity	Core Nozzle Plug Material Density	lb/in3	0.160	0.159	0.161	10	10	
258	Core_Nozz_Wate_plugThickness	Core Nozzle Plug Thickness	in	0.060	0.060	0.060	10	10	

Continued on Next Page...

Table A.1 – Continued

	Input Name	Input Description	Units	Baseline Value	Minimum	Maximum	α	β	Held Constant
259	Byp_Nozz_Cv	Bypass Nozzle Exit Velocity Loss Coefficient		0.998	0.990	0.998	2	1	
260	Byp_Nozz_Wate_LDratio	Bypass Nozzle Length to Diameter Ratio		0.435	0.428	0.442	10	10	
261	Byp_Nozz_Wate_exitOuterRadius	Bypass Nozzle Exit Outer Radius		61.00	60.09	61.92	10	10	Yes
262	k_Byp_Wt	Bypass Nozzle Weight Adjustment Factor		0.000	-0.004	0.004	10	10	
263	Byp_Nozz_Wate_nozzleDensity	Bypass Nozzle Material Density	lb/in3	0.100	0.100	0.100	10	10	
264	HP_Shaft_Nmech	High Pressure Shaft Mechanical Speed		9041.70	8906.07	9177.33	10	10	
265	HP_Shaft_HPX	High Pressure Shaft Horse Power Extraction	hp	243.00	239.36	246.65	10	10	
266	HP_Shaft_Wate_limitStress	High Pressure Shaft Stress Limit	psia	50000	49250	50750	10	10	
267	HP_Shaft_Wate_diamRatio	High Pressure Shaft Inner to Outer Diameter Ratio		0.833	0.821	0.845	10	10	Yes
268	k_HP_Wt	High Pressure Shaft Weight Adjustment Factor		0.000	0.000	0.000	10	10	Yes
269	HP_Shaft_Wate_density	High Pressure Shaft Material Density	lb/in3	0.300	0.299	0.301	10	10	
270	LP_Shaft_Nmech	Low Pressure Shaft Mechanical Speed		2768.20	2726.68	2809.72	10	10	
271	LP_Shaft_Wate_limitStress	Low Pressure Shaft Stress Limit	psia	50000	49250	50750	10	10	
272	LP_Shaft_Wate_diamRatio	Low Pressure Shaft Diameter Ratio		0.833	0.821	0.845	10	10	
273	k_LP_Wt	Low Pressure Shaft Weight Adjustment Factor		0.000	0.000	0.000	10	10	Yes
274	LP_Shaft_Wate_density	Low Pressure Shaft Material Density	lb/in3	0.287	0.286	0.288	10	10	
275	Velocity_Ratio_eq_rhs	Exit Velocity Ratio		1.461	1.439	1.483	10	10	
276	PERF_k_Fgbase	Thrust Scaling Factor		1.000	0.985	1.015	10	10	
277	k_LPC_loading	LPC Loading Adjustment Factor		0.000	-0.015	0.015	10	10	
278	LPT_LPC_ratio	LPT to LPC Diameter Ratio		0.920	0.906	0.934	10	10	Yes
279	CoreNozz_LPT_ratio	Core Nozzle to LPT Radius Ratio		0.950	0.936	0.964	10	10	
280	BypassNozz_Fan_ratio	Bypass Nozzle Exit Location Factor		3.000	2.955	3.045	10	10	
281	VMMO	Maximum operating Mach number		0.870	0.857	0.883	10	10	
282	DIH	Wing Dihedral	deg	6.000	5.910	6.090	10	10	
283	FLAPR	Flap to Wing Area Ratio		0.219	0.216	0.222	10	10	
284	XL	Fuselage total length	ft	209.10	205.96	212.24	10	10	
285	WF	Maximum fuselage width	ft	20.33	20.03	20.63	10	10	
286	DF	Maximum fuselage depth	ft	20.33	20.03	20.63	10	10	
287	XLP	Length of passenger compartment	ft	161.08	158.66	163.50	10	10	
288	XMLG	Length of extended main landing gear oleo	in	89.58	88.24	90.92	10	10	
289	XNLG	Length of extended nose landing gear oleo	in	96.10	94.66	97.54	10	10	
290	SHT	Horizontal tail theoretical area	ft2	1109.92	1093.27	1126.57	10	10	
291	SWPHT	Horizontal tail 25% chord sweep angle	deg	55.00	54.18	55.83	10	10	Yes
292	ARHT	Horizontal tail theoretical aspect ratio		4.580	4.511	4.649	10	10	
293	TRHT	Horizontal tail theoretical taper ratio		0.330	0.325	0.335	10	10	
294	TCHT	Thickness-chord ratio for the horizontal tail		0.080	0.079	0.081	10	10	
295	SVT	Vertical tail theoretical area	ft2	676.04	665.90	686.18	10	10	

Continued on Next Page...

Table A.1 – Continued

	Input Name	Input Description	Units	Baseline Value	Minimum	Maximum	α	β	Held Constant
296	SWPVT	Vertical tail 25% chord sweep angle	deg	50.00	49.25	50.75	10	10	Yes
297	ARVT	Vertical tail theoretical aspect ratio		1.780	1.753	1.807	10	10	
298	TRVT	Vertical tail theoretical taper ratio		0.250	0.246	0.254	10	10	
299	TCVT	Vertical-chord ratio for the horizontal tail		0.090	0.089	0.091	10	10	
300	NPF	Number of first class passengers		30.00	29.00	31.00	2	2	
301	NPT	Number of tourist passengers		271.00	266.00	276.00	2	2	
302	WPPASS	Weight per passenger	lb	185.00	182.23	187.78	10	10	
303	BPP	Weight of baggage per passenger	lb	35.00	34.48	35.53	10	10	
304	NFLCR	Number of flight crew		2.000	1.000	3.000	2	2	
305	FRWI	Scaling Factor - Total wing weight		1.000	0.985	1.015	10	10	
306	FRFU	Scaling Factor Fuselage weight		1.300	1.281	1.320	10	10	
307	FRHT	Scaling Factor Horizontal tail weight		1.150	1.133	1.167	10	10	
308	FRVT	Scaling Factor Vertical tail weight		1.150	1.133	1.167	10	10	
309	FRLGM	Scaling Factor Landing gear weight, main		1.150	1.133	1.167	10	10	
310	FRSC	Scaling Factor Surface controls weight		1.300	1.281	1.320	10	10	
311	WFURN	Scaling Factor Furnishings Group weight		1.300	1.281	1.320	10	10	
312	WHYD	Scaling Factor Hydraulics Group weight		1.150	1.133	1.167	10	10	
313	WAVONC	Scaling Factor Avionics Group weight		1.150	1.133	1.167	10	10	
314	WELEC	Scaling Factor Electrical Group weight		1.200	1.182	1.218	10	10	
315	WFSYS	Scaling Factor - Weight of fuel system		1.150	1.133	1.167	10	10	
316	WAPU	Scaling Factor Auxiliary power unit weight		1.150	1.133	1.167	10	10	
317	WIN	Scaling Factor Instrument Group weight		1.200	1.182	1.218	10	10	
318	WAI	Scaling Factor Anti-icing Group weight		1.000	0.985	1.015	10	10	
319	FULWMX	Scaling Factor Total fuel capacity of wing		22.00	21.67	22.33	10	10	Yes
320	FULFMX	Total fuel capacity of fuselage	lb	95000	93575	96425	10	10	Yes
321	DESRNG	Design range	nmi	8100	7979	8222	10	10	
322	VCMN	Cruise Mach number		0.840	0.827	0.853	10	10	
323	CH	Maximum cruise altitude	ft	43000	42355	43645	10	10	
324	GW	Ramp weight	lb	656000	646160	665840	10	10	
325	TR	Taper ratio of the wing		0.140	0.138	0.142	10	10	
326	SWEEP	Quarter-chord sweep angle of the wing	deg	31.00	30.54	31.47	10	10	
327	TCA	Wing thickness-chord ratio (weighted average)		0.10	0.10	0.11	10	10	
328	AR	Wing aspect ratio		8.70	8.57	8.83	10	10	
329	TWR	required total thrust-weight ratio		0.26	0.26	0.27	10	10	
330	SW	Reference wing area	ft2	4605.0	4535.9	4674.1	10	10	
331	AITEK	Airfoil technology parameter		1.880	1.852	1.908	10	10	
332	CLTOM	Maximum CL in takeoff configuration		2.000	1.970	2.030	10	10	

Continued on Next Page...

Table A.1 – Continued

	Input Name	Input Description	Units	Baseline Value	Minimum	Maximum	α	β	Held Constant
333	CLLDM	Maximum CL in landing configuration		3.000	2.955	3.045	10	10	
334	TAKOTM	Takeoff time	min	2.000	1.970	2.030	10	10	
335	TAXOTM	Taxi out time	min	9.000	8.865	9.135	10	10	
336	APPRTM	Approach time	min	4.000	3.940	4.060	10	10	
337	TAXITM	Taxi in time	min	5.000	4.925	5.075	10	10	
338	RCIN	Instantaneous rate of climb for ceiling calculation	ft/min	300.0	295.5	304.5	10	10	Yes
339	CRALT	Maximum or fixed altitude	ft	42000	41370	42630	10	10	
340	TIMMAP	Missed approach time	min	2.000	1.970	2.030	10	10	Yes
341	RESTRP	Reserve fuel as a fraction of total trip fuel weight		0.050	0.049	0.051	10	10	
342	FCDI	Lift-dependent Drag Coefficients Factor		1.000	0.985	1.015	10	10	
343	FCDO	Lift-independent Drag Coefficients Factor		1.000	0.985	1.015	10	10	
344	CONALT	Altitude at which constraint is to be evaluated	ft	35000	34475	35525	10	10	Yes
345	CONMCH	Velocity at which constraint is to be evaluated		0.840	0.827	0.853	10	10	Yes
346	APRHGT	Height above ground for start of approach	ft	3010.0	2964.9	3055.2	10	10	
347	RVFACT	Fraction of thrust reversed - net		-0.400	-0.394	-0.406	10	10	Yes
348	WHGT	Wing height above ground	ft	12.00	11.82	12.18	10	10	
349	BRAKMU	Coefficient of friction, brakes on		0.400	0.394	0.406	10	10	Yes
350	VANGL	Rotation rate	deg/sec	2.500	2.463	2.538	10	10	
351	CDGEAR	Landing gear drag coefficient		0.005	0.005	0.005	10	10	
352	CDEOUT	Engine Out Delta Drag		0.005	0.005	0.005	10	10	
353	CLSPOL	Spoiler delta lift coefficient		-0.500	-0.493	-0.508	10	10	Yes
354	CDSPOL	Spoiler delta drag coefficient		0.050	0.049	0.051	10	10	Yes
355	cltom	Maximum CL in takeoff configuration		3.150	3.103	3.197	10	10	
356	ALMXTO	Maximum angle of attack during takeoff	deg	13.00	12.81	13.20	10	10	
357	ALPROT	Maximum angle of attack during rotation	deg	13.00	12.81	13.20	10	10	Yes
358	TIGEAR	Time required to retract landing gear	s	9.000	8.865	9.135	10	10	
359	break_loc	Location of wing breakpoint		0.268	0.264	0.272	10	10	
360	t_c_root	Wing root thickness-chord ratio		0.128	0.126	0.130	10	10	
361	t_c_tip	Wing tip thickness-chord ratio		0.080	0.079	0.081	10	10	
362	D_Oper_M	Operational Mach delta		0.000	-0.015	0.015	10	10	
363	k_Oper_R	Operational Range multiplier		0.370	0.365	0.376	10	10	
364	k_Oper_Payload	Global Variable		0.510	0.502	0.518	10	10	
365	Fan_In_CB	Fan inlet noise at cutback		0.000	-0.066	0.065	10	10	
366	Fan_In_AP	Fan inlet noise at approach		0.000	-0.066	0.065	10	10	
367	Fan_In_SL	Fan inlet noise at sideline		0.000	-0.066	0.065	10	10	
368	Fan_Ex_CB	Fan exhaust noise at cutback		0.000	-0.066	0.065	10	10	
369	Fan_Ex_AP	Fan exhaust noise at approach		0.000	-0.066	0.065	10	10	

Continued on Next Page...

Table A.1 – Continued

	Input Name	Input Description	Units	Baseline Value	Minimum	Maximum	α	β	Held Constant
370	Fan_Ex_SL	Fan exhaust noise at sideline		0.000	-0.066	0.065	10	10	
371	Jet_CB	Total jet noise at cutback		0.000	-0.066	0.065	10	10	
372	Jet_AP	Total jet noise at approach		0.000	-0.066	0.065	10	10	
373	Jet_SL	Total jet noise at sideline		0.000	-0.066	0.065	10	10	
374	Slat_AP	Wing slat noise at approach		0.000	-0.066	0.065	10	10	
375	Flap_AP	Wing flap noise at approach		0.000	-0.066	0.065	10	10	
376	LG_AP	Landing gear noise at approach		0.000	-0.066	0.065	10	10	
377	k_Str_payload	Delta (in percent) from max structural payload		1.140	1.123	1.157	10	10	
378	k_CL_TO	Delta CL at Takeoff		0.000	-0.015	0.015	10	10	
379	k_CD_TO	Delta CD at Takeoff		0.000	-0.002	0.002	10	10	
380	k_CL_Ldg	Delta CL at Landing		0.000	-0.015	0.015	10	10	
381	k_CD_Ldg	Delta CD at Landing		0.000	-0.002	0.002	10	10	

Bibliography

[1] Aircraft Engine Emissions Database. June 2006. http://www.caa.co.uk/default.aspx?categoryid=702&pagetype=90.

[2] Federal Aviation Administration Type Certificate Data Sheet. May 2006. http://www.airweb.faa.gov/Regulatory_and_Guidance_Library/rgMakeModel.nsf.

[3] Federal Aviation Regulations. July 2006. http://www.airweb.faa.gov/Regulatory_and_Guidance_Library/rgFAR.nsf.

[4] NIST/SEMATECH e-Handbook of Statistical Methods, October 2006. http://www.itl.nist.gov/div898/handbook/.

[5] Baghdasaryan, Lusine and Chen, Wei and Buranathiti, Thaweepat and Cao, Jian. Model Validation via Uncertainty Propagation using Response Surface Models. Technical Report DETC2002/DAC-34140, October 2002.

[6] G. L. Converse and R. G. Giffin. Extended Parametric Representation of Compressor Fans and Turbines. Volume 1 CMGEN User Manual. Technical Report NASA CR-174645, General Electric Aircraft Engine Group, Cleveland, Ohio, March 1984.

[7] G. L. Coverse. Extended Parametric Representation of Compressor Fans and Turbines. Volume 2 PART User Manual. Technical Report NASA CR-174646, General Electric Aircraft Engine Group, Cleveland, Ohio, March 1984.

[8] G. L. Coverse. Extended Parametric Representation of Compressor Fans and Turbines. Volume 3 MODFAN User Manual. Technical Report NASA CR-174647, General Electric Aircraft Engine Group, Cleveland, Ohio, March 1984.

[9] David L. Daggett. Ultra Efficient Engine Technology Systems Integration and Environmental Assessment. Technical Report NASA CR-2002-211754, Boeing Commercial Airplane Group, Seattle, Washington, July 2002.

[10] Department of Defense. DoD Modeling and Simulation (M&S) Glossary. Technical Report DoD Directive 5000.59, Department of Defense, Washington, D.C., January 1998.

[11] R. C. Feagin. Delta Method, An Empirical Drag Buildup Technique. Technical Report NASA CR-151971, Lockheed, Burbank, California, December 1978.

[12] Lawrence L. Green. Probablistic Methods for Uncertainty Propagation Applied to Aircraft Design. Technical Report AIAA 2002-3140, NASA Langley Research Center, Hampton, Virginia, June 2002.

[13] Bill Gunston and Jane's Information Group. *Jane's Aero-engines.* Jane's Information Group, Alexandria, VA, 2000.

[14] George A. Hazelrigg. Thoughts on Model Validation for Engineering Design. Technical Report DETC2003/DTM-48632, National Science Foundation, Arlington, Virginia, September 2003.

[15] Marcus F. Heidmann. Interim Prediction Method for Fan and Compressor Source Noise. Technical Report NASA-TM-X-71763, Lewis Research Center, Cleveland, Ohio, June 1975.

[16] Peter Hollingsworth, Dimitri Mavris, and Ian Waitz. Vehicle Systems Program Assessment Environment Overview and Differences to EDS Version 1.0. Georgia Institute of Technology and Massachusetts Institute of Technology, 2006.

[17] IEEE Computer Society. IEEE Standard for Software Verification and Validation. Technical Report IEEE Std 1012-2004, Institute of Electrical and Electronics Engineers, New York, New York, June 2004.

[18] Michelle R. Kirby. An Overview of Response Surface Methodology. Georgia Institute of Technology, 2006.

[19] Michelle R. Kirby. The Beginner's Guide to Fitting Response Surfaces. Georgia Institute of Technology, 2006.

[20] Richard Klein, Scott Doebling, Frank Graziani, Marty Pilch, and Tim Trucano. ASC Perdictive Science Academic Alliance Program Verification and Validation Whitepaper. Technical Report UCRL-TR-220711, March 2006.

[21] K. B. Kontos, B. A. Janardan, and P. R. Gliebe. Improved NASA-ANOPP Noise Prediction Computer Code for Advanced Subsonic Propulsion Systems. Technical Report NASA CR-195480, GE Aircraft Engines, Cincinnati, Ohio, August 1996.

[22] L. A. McCullers. *Flight Optimization System User's Guide Release 6.12.* NASA Langley Research Center, Hampton, Virginia, October 2004.

[23] L. A. McCullers. *TAKEOFF Detailed Takeoff and Landing Analysis Program User's Guide.* NASA Langley Research Center, Hampton, Virginia, October 2004.

[24] NASA Glenn Research Center, Cleveland, Ohio. *NPSS User Guide*, May 2004.

[25] Roger D. Schaufele. *The Elements of Aircraft Preliminary Design.* Aries Publications, Santa Ana, CA, 2000.

[26] Marian E. Scott. Uncertainty and Sensitivity Studies of Models of Environmental Systems. Technical Report Proceedings of hte 1996 Winter Simulation Conference, University of Glasgow, Glasgow, United Kingdom, 1996.

[27] Ben H. Thacker, David S. Riha, Harry R. Millwater, and Michael P. Enright. Errors and Uncertainty in Probabilistic Engineering Analysis. Technical Report AIAA 2001-1239, Southwest Research Institute, San Antonio, Texas, April 2001.

[28] Timothy G. Trucano. Prediction and Uncertainty in Computational Modeling of Complex Phenomena: A Whitepaper. Technical Report SAND98-2776, Sandia National Laboratories, Albuquerque, New Mexico, December 1998.

[29] Ian Waitz, Stephen Lukachko, Karen Willcox, Peter Belobaba, Elena Garcia, Peter Hollingsworth, Dimitri Mavris, Kate Harback, Fred Morser, and Michele Steinbach. Architecture Study for the Aviation Environmental Portfolio Management Tool. June 2006.